Millisecond $23/2^+$ isomers in the $N = 79$ isotones ^{133}Xe and ^{135}Ba

L. Kaya,[1,*] A. Vogt,[1] P. Reiter,[1] C. Müller-Gatermann,[1] M. Siciliano,[2,3] L. Coraggio,[4] N. Itaco,[4,5] A. Gargano,[4] K. Arnswald,[1] D. Bazzacco,[6] B. Birkenbach,[1] A. Blazhev,[1] A. Bracco,[7] B. Bruyneel,[8] L. Corradi,[3] F. C. L. Crespi,[7] G. de Angelis,[3] M. Droste,[1] J. Eberth,[1] E. Farnea,[6,†] E. Fioretto,[3] C. Fransen,[1] A. Gadea,[9] A. Giaz,[7] A. Görgen,[10,11,12] A. Gottardo,[3] K. Hadyńska-Klęk,[3] H. Hess,[1] R. Hetzenegger,[1] R. Hirsch,[1] P. R. John,[13] J. Jolie,[1] A. Jungclaus,[14] W. Korten,[11] S. Leoni,[7] L. Lewandowski,[1] S. Lunardi,[2,6] R. Menegazzo,[6] D. Mengoni,[15,2,6] C. Michelagnoli,[16] T. Mijatović,[17] G. Montagnoli,[2,6] D. Montanari,[18] D. Napoli,[3] Zs. Podolyák,[19] G. Pollarolo,[20] F. Recchia,[2,6] D. Rosiak,[1] N. Saed-Samii,[1] E. Şahin,[10] F. Scarlassara,[2,6] M. Seidlitz,[1] P.-A. Söderström,[13] A. M. Stefanini,[3] O. Stezowski,[21] S. Szilner,[17] B. Szpak,[22] C. Ur,[6] J. J. Valiente-Dobón,[3] M. Weinert,[1] K. Wolf,[1] and K. O. Zell[1]

[1]*Institut für Kernphysik, Universität zu Köln, D-50937 Köln, Germany*
[2]*Dipartimento di Fisica e Astronomia, Università di Padova, I-35131 Padova, Italy*
[3]*Istituto Nazionale di Fisica Nucleare, Laboratori Nazionali di Legnaro, I-35020 Legnaro, Italy*
[4]*Istituto Nazionale di Fisica Nucleare, Sezione di Napoli, I-80126 Napoli, Italy*
[5]*Dipartimento di Matematica e Fisica, Università degli Studi della Campania "Luigi Vanvitelli", viale A. Lincoln 5, I-8110 Caserta, Italy*
[6]*Istituto Nazionale di Fisica Nucleare, Sezione di Padova, I-35131 Padova, Italy*
[7]*Dipartimento di Fisica, Università di Milano and INFN Sezione di Milano, I-20133 Milano, Italy*
[8]*CEA Saclay, Service de Physique Nucleaire, F-91191 Gif-sur-Yvette, France*
[9]*Instituto de Física Corpuscular, CSIC-Universidad de Valencia, E-46071 Valencia, Spain*
[10]*Department of Physics, University of Oslo, P. O. Box 1048 Blindern, N-0316 Oslo, Norway*
[11]*Institut de Recherche sur les lois Fondamentales de l'Univers – IRFU, CEA/DSM, Centre CEA de Saclay, F-91191 Gif-sur-Yvette Cedex, France*
[12]*Lawrence Berkeley National Laboratory, Berkeley, California 94720, USA*
[13]*Institut für Kernphysik, Technische Universität Darmstadt, D-64289 Darmstadt, Germany*
[14]*Instituto de Estructura de la Materia, CSIC, Madrid, E-28006 Madrid, Spain*
[15]*Nuclear Physics Research Group, University of the West of Scotland, High Street, Paisley PA1 2BE, Scotland, United Kingdom*
[16]*Institut Laue-Langevin (ILL), 38042 Grenoble Cedex 9, France*
[17]*Ruđer Bošković Institute, HR-10 002 Zagreb, Croatia*
[18]*USIAS - Universite de Strasbourg, IPHC-CNRS, F-67037 Strasbourg Cedex 2, France*
[19]*Department of Physics, University of Surrey, Guildford, Surrey GU2 7XH, United Kingdom*
[20]*Dipartimento di Fisica Teorica dell'Università di Torino and INFN, I-10125 Torino, Italy*
[21]*Université de Lyon, Université Lyon-1, CNRS/IN2P3, UMR5822, IPNL, F-69622 Villeurbanne Cedex, France*
[22]*Henryk Niewodniczański Institute of Nuclear Physics PAN, PL-31342 Kraków, Poland*

(Received 27 July 2018; published 19 November 2018)

Detailed information on isomeric states in $A \approx 135$ nuclei is exploited to benchmark shell-model calculations in the region northwest of doubly magic nucleus ^{132}Sn. The $N = 79$ isotones ^{133}Xe and ^{135}Ba are studied after multinucleon transfer in the ^{136}Xe + ^{208}Pb reaction employing the high-resolution Advanced GAmma Tracking Array (AGATA) coupled to the magnetic spectrometer PRISMA at the Laboratori Nazionali di Legnaro, Italy and in a pulsed-beam experiment at the FN tandem accelerator of the University of Cologne, Germany utilizing a ^{9}Be + ^{130}Te fusion-evaporation reaction at a beam energy of 40 MeV. Isomeric states are identified via delayed γ-ray spectroscopy. Hitherto tentative excitation energy, spin, and parity assignments of the 2107-keV $J^\pi = 23/2^+$ isomer in ^{133}Xe are confirmed and a half-life of $T_{1/2} = 8.64(13)$ ms is measured. The 2388-keV state in ^{135}Ba is identified as a $J^\pi = 23/2^+$ isomer with a half-life of 1.06(4) ms. The new results show a smooth onset of isomeric $J^\pi = 23/2^+$ states along the $N = 79$ isotones and close a gap in the high-spin systematics towards the recently investigated $J^\pi = 23/2^+$ isomer in ^{139}Nd. The resulting systematics of $M2$ reduced transition probabilities is discussed within the framework of the nuclear shell model. Latest large-scale shell-model calculations employing the SN100PN, GCN50:82, SN100-KTH, and a realistic effective interaction reproduce the experimental findings generally well and give insight into the structure of the isomers.

DOI: 10.1103/PhysRevC.98.054312

*Corresponding author: levent.kaya@ikp.uni-koeln.de
†Deceased.

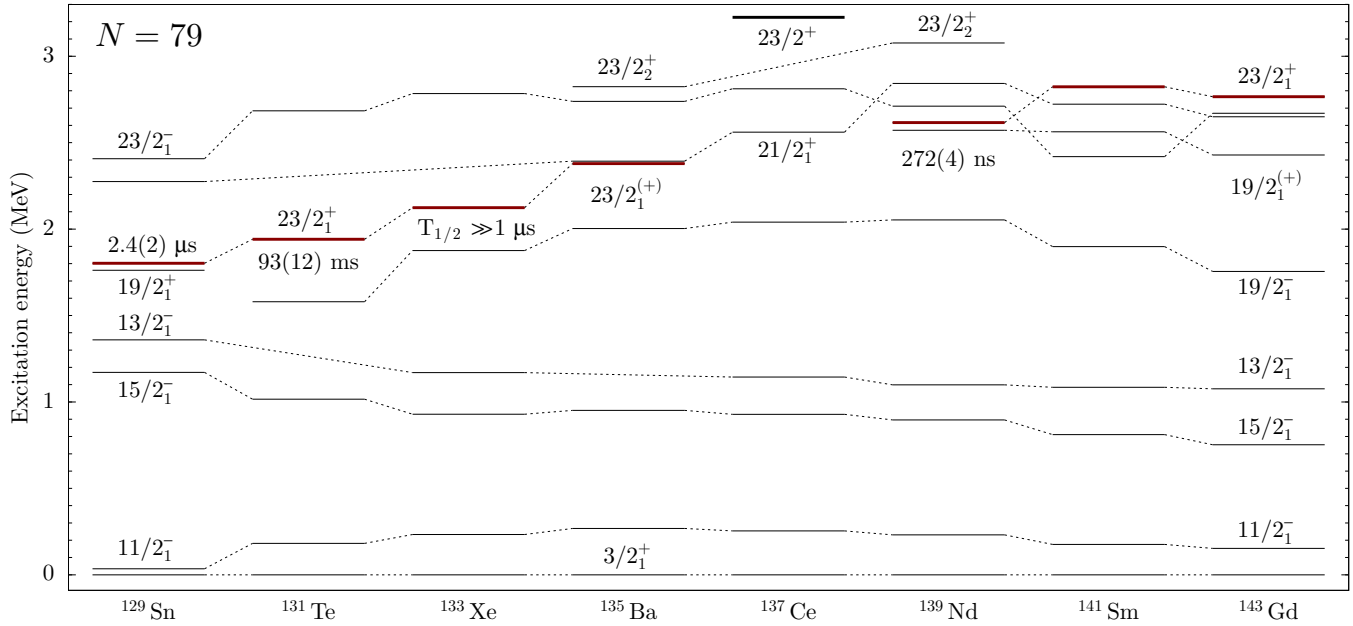

FIG. 1. Evolution of excited states along the $N = 79$ chain. Dashed lines connecting levels of same spin and parity are drawn to guide the eye. The $J^\pi = 23/2^+_1$ states in ^{129}Sn, ^{131}Te, and ^{139}Nd are isomers. A candidate for a $J^\pi = 23/2^+$ isomer at $E_x = 2107 + x$ keV was reported in ^{133}Xe [5]. It is expected that a corresponding long-lived state is also present in ^{135}Ba. Data extracted from the ENSDF database [8] and Refs. [1,5–7].

I. INTRODUCTION

The $N = 79$ isotones ^{133}Xe and ^{135}Ba, only three neutrons away from the $N = 82$ shell closure, are located within the proton midshell between the $Z = 50$ shell and the $Z = 64$ subshell closures. In this region, the evolution of nuclear collectivity competes with the excitation of single-particle states. Enabling high-j couplings, the intruder $h_{11/2}$ neutron orbital is pivotal for high-spin states in this region. ^{133}Xe and ^{135}Ba present an intriguing study ground for the predictive power of the shell model at both low and high spins in the vicinity of the $N = 82$ neutron closed shell. In particular, detailed knowledge of long-lived states—so-called isomers—provide a sensitive probe for the active quasiparticle configurations.

Figure 1 shows the evolution of several negative-, and positive-parity states along the $N = 79$ chain, ranging from semimagic $^{129}_{50}$Sn up to $^{143}_{64}$Gd. Isomeric $J^\pi = 11/2^-_1$ states with neutron-hole $\nu h^{-1}_{11/2}$ configurations were discovered in all odd-mass $N = 79$ isotones. Furthermore, several $J^\pi = 19/2^+$, $23/2^+$, and $27/2^-$ high-spin isomers above the $J^\pi = 11/2^-_1$ states were reported in the literature. These isomeric states are explained as high-spin members of the $\nu(h^{-2}_{11/2}d^{-1}_{3/2})$ and $\nu(h^{-n}_{11/2})$, seniority $v = 3$ multiplets [1–9].

Information on excited states in ^{129}Sn and ^{131}Te were mainly obtained from β decay and actinide fission studies. In a previous experiment, the semimagic nucleus ^{129}Sn was populated via thermal neutron-induced fission and investigated by means of γ-ray and electron-conversion spectroscopy [1,9]. Two L conversion lines corresponding to transition energies of 41.0 and 19.7 keV were identified as the decay of $J^\pi = 23/2^+$ and $19/2^+$ states, respectively. Based on the decay curves of the two electron-conversion lines and corresponding γ-ray decays, half-lives of $T_{1/2} = 2.4(2)$ μs for the $J^\pi = 23/2^+$ state and $T_{1/2} = 3.6(2)$ μs for the $J^\pi = 19/2^+$ state were determined [1]. In ^{129}Sn the seniority $v = 3$ multiplet is completed by the $J^\pi = (27/2^-)$ state at $E_x = 2552$ keV [$T_{1/2} = 0.27(7)$ μs], identified by Lozeva *et al.* in 2008 [4].

^{131}Te was populated in a pioneering ^{64}Ni + ^{130}Te multinucleon-transfer experiment at the GASP γ-ray spectrometer [10]. A delayed 361-564-833-keV triple-γ coincidence was identified to form the $(21/2^-) \rightarrow (19/2^-) \rightarrow (15/2^-) \rightarrow 11/2^-$ yrast band. Referring to isotopic systematics, a $J^\pi = 23/2^+$ isomer is proposed that is located slightly above the $J^\pi = (21/2^-)$ state at $E_x = 1941$ keV with a lower half-life limit of $T_{1/2} > 1$ μs. However, no low-energy $E1$ transition was observed in this work. Soon after, ^{131}Te was also populated after thermal fission of U isotopes at the OSIRIS mass separator by Fogelberg *et al.* [6]. In this work, a very long half-life of $T_{1/2} = 93(12)$ ms was determined. Based on conversion-electron measurements, the authors excluded a low-energy $E1$ transition hypothesis and the $E_x = 1941$-keV state was revised to be a $J^\pi = (23/2^+)$ isomer. The 361-keV transition was proposed to be of $E3$ character, connecting the isomer with a $J^\pi = (17/2^-)$ state. Finally, in a later fusion-fission experiment by Astier *et al.* [2] utilizing the EUROBALL array, the negative-parity band on top of the $J^\pi = (19/2^-)$ state was extended to excitation energies of approximately 4.7 MeV and spin $J^\pi = (35/2^-)$. The determined lower limit of the half-life of the $J^\pi = (23/2^+)$ state ($T_{1/2} \gg 10$ μs) is in agreement with the previous experiment. The multipolarity of the 361-keV transition was reevaluated to be mainly of $M2$ character. Based on the OSIRIS result and the reevaluated $M2$ character, a reduced transition strength of $B(M2; 23/2^+_1 \rightarrow 19/2^-_1) = 2.0(3) \times 10^{-6}$ W.u. [2] was

deduced. Shell-model calculations predict a $\nu(h_{11/2}^{-2}d_{3/2}^{-1})$ configuration for the $J^\pi = (23/2^+)$ state and a predominant $(\nu h_{11/2}^{-1})(\pi g_{7/2}^2)$ configuration for the $J^\pi = (19/2^-)$ state. No feeding transitions for the $J^\pi = (23/2^+)$ isomer were yet discovered in ^{131}Te.

Going to the proton midshell, a first search of high-spin isomers in ^{137}Ce was made using a ^{4}He + ^{138}Ba reaction [11]. No evidence for a long-lived state was found in the off-beam range from 10–300 μs with respect to the beam pulse. Later, a $J = (31/2)$ state at $E_x = 4255$ keV was observed to be isomeric with a half-life of $T_{1/2} = 5(2)$ ns according to the time distribution of the depopulating 552-keV γ ray [12]. The level scheme of ^{137}Ce was extended up to highest spins via ^{18}O + ^{124}Sn [13] and ^{13}C + ^{130}Te [14] reactions. To date, only a $J^\pi = 23/2^+$ state above $E_x = 3$ MeV is reported. It is much higher in excitation energy than in the other $N = 79$ isotones and disrupts the systematics (c.f. Fig. 1).

First spectroscopic data on the elusive $J^\pi = 23/2^+$ isomer in ^{139}Nd were reported by Müller-Veggian *et al.* [15] employing a ^{140}Ce$(\alpha, 5n)$ reaction. The level scheme above the $J^\pi = 11/2_1^-$ isomer was extended to an excitation energy of approximately 4 MeV. Delayed γ rays deexciting the $J^\pi = 19/2_1^+$ state were observed in off-beam $\gamma\gamma$-coincidence spectra. Based on the decay curve, a half-life limit of $T_{1/2} >$ 141 ns was deduced. Later, the isomer's excitation energy was constrained to be above the $J^\pi = 19/2_1^+$ state and a precise half-life of $T_{1/2} = 272(4)$ ns could be obtained [7]. However, the isomer could not unambiguously place in the level scheme. Finally, in 2013, a recoil-decay tagging experiment at the Jyväskylä accelerator facility confirmed the previous half-life measurement [3]. The authors observed feeding transitions from the decay of three higher-lying $J^\pi = (25/2^-)$ states allowing for a placement of the isomeric $J^\pi = (23/2^+)$ state in the level scheme at $E_x = 2616$ keV, only 44 keV above the $J^\pi = 19/2^+$ state. However, that 44-keV transition is still unobserved. Towards the subshell closure at $Z = 64$, detailed high-spin structure information is available for ^{141}Sm [16,17] and ^{143}Gd [17–19]; no high-lying isomeric states were observed.

The onset of isomerism as a function of the proton number along the $N = 79$ chain (see Fig. 1) motivates a refined investigation of isomeric $J^\pi = 23/2^+$ states in ^{133}Xe and ^{135}Ba. The available data on low-spin states in ^{133}Xe mainly originate from β-decay studies of ^{133}I [20]. The $J^\pi = 11/2_1^-$ isomer at 233 keV with a $\nu h_{11/2}^{-1}$ neutron-hole configuration has a half-life of 2.198(13) d [21]. First results on the high-spin structure were obtained by Lönnroth *et al.* [22] via α-induced reactions on ^{130}Te at beam energies of 14.1–18 MeV. Three γ rays with energies of 247.4, 947.8, and 695.2 keV were placed above the $J^\pi = 11/2_1^-$ isomer to form a $(23/2^-) \rightarrow 19/2_1^- \rightarrow 15/2_1^- \rightarrow 11/2_1^-$ cascade.

Recently, the high-spin regime of ^{133}Xe was extended via ^{136}Xe + ^{208}Pb and ^{136}Xe + ^{198}Pt multinucleon-transfer reactions employing the Advanced GAmma Tracking Array (AGATA) coupled to the magnetic spectrometer PRISMA and the GAMMASPHERE spectrometer in combination with the gas-filled detector array CHICO, respectively [5]. A 1253-468-465-keV prompt triple coincidence was observed to form a band unconnected to any known states in ^{133}Xe. According to the time structure in the GAMMASPHERE data set, a long-lived isomer with $T_{1/2} \gg 1$ μs was proposed at $E_x = 2107 + x$ keV.

High-spin states in ^{135}Ba above the $J^\pi = 11/2_1^-$ isomer ($T_{1/2} = 28.7$ h [23]) were investigated by Che *et al.* [24]. Excited states were populated up to excitation energies of 5.8 MeV using a ^{130}Te(^{9}Be, $4n$)^{135}Ba reaction at 45 MeV. A 1184-254 keV cascade was observed to feed the $J^\pi = 15/2_1^-$ state at $E_x = 950$ keV. The 2134-keV state was identified as the $J^\pi = 19/2_2^-$ state, while no spin assignment was given for the 2388-keV state. Moreover, no decay from higher-lying states into the 2388-keV state was observed. Later, a first tentative spin assignment of $J^\pi = 21/2^{(-)}$ was proposed for the 2388-keV state [25]. A high-spin investigation by Kumar *et al.* extended the level scheme with 20 new γ rays [26]. Directional correlation measurements confirmed the spin and parity assignments of the $J^\pi = 19/2_2^-$ state and indicated a tentative $J = (23/2)$ spin assignment for the 2388-keV state. Even though detailed data are available up to highest spins and excitation energies, no feeding γ ray to the 2388-keV state was found to date. This observation corroborates the existence of a long-lived $J = 23/2_1^+$ isomer in ^{135}Ba.

In this paper, we report and discuss new results on isomeric $J^\pi = 23/2^+$ states in the $N = 79$ isotones ^{133}Xe and ^{135}Ba obtained in two different experiments. ^{135}Ba was populated in a ^{136}Xe + ^{208}Pb multinucleon-transfer (MNT) experiment employing the high-resolution position-sensitive Advanced GAmma Tracking Array (AGATA) [27] in combination with the magnetic mass spectrometer PRISMA [28–30]. In a fusion-evaporation experiment, both ^{133}Xe and ^{135}Ba were investigated with the HORUS γ-ray array [31] at the Institute of Nuclear Physics, University of Cologne, employing a pulsed 40-MeV ^{9}Be beam impinging onto a ^{130}Te target. This paper is organized as follows: the experimental setup and data analysis of the two experiments are described in Sec. II, followed by the experimental results in Sec. III. A detailed comparison with shell-model calculations is presented in Sec. IV before the paper closes with a summary and conclusions.

II. EXPERIMENTAL PROCEDURE AND DATA ANALYSIS

A. ^{136}Xe + ^{208}Pb multinucleon transfer

^{135}Ba was populated in a ^{136}Xe + ^{208}Pb multinucleon-transfer experiment at the Laboratori Nazionali di Legnaro, Italy. In this experiment, a 6.84 MeV/nucleon ^{136}Xe beam, accelerated by the PIAVE+ALPI accelerator complex, impinged onto a 1-mg/cm^2 ^{208}Pb target. The Advanced GAmma Tracking Array (AGATA) [27] in a first demonstrator configuration [32] was placed at a distance of 18.8 cm from the target position to measure γ rays from excited states. The array consisted of nine large-volume electronically segmented high-purity Ge (HPGe) detectors in three triple cryostats [33]. An isotopic identification of the nuclei of interest was provided by the magnetic spectrometer PRISMA placed at the reaction's grazing angle of $\theta_{\rm lab} = 42^\circ$. An event registered by the PRISMA focal-plane detector in coincidence with an AGATA event was taken as a trigger for the data acquisition.

Pulse-shape analysis of the digitized detector signals was applied to determine the individual interaction points within the HPGe shell [34], enabling the Orsay forward-tracking algorithm [35] to reconstruct the individual emitted γ-ray energies, determine the first interaction point of the γ ray in the germanium and, thus, the emission angle. Together with the kinematic information from PRISMA, a precise Doppler correction was performed. Further details on the analysis can be found in Refs. [36,37].

B. ^{9}Be + ^{130}Te fusion-evaporation reaction

In a second experiment, ^{133}Xe and ^{135}Ba were populated in a ^{130}Te + ^{9}Be fusion-evaporation reaction. The FN Tandem accelerator of the Institute of Nuclear Physics, University of Cologne delivered pulsed 40-MeV ^{9}Be beams with two different repetition rates onto an enriched ^{130}Te target with a thickness of 1.8 mg/cm^2 evaporated onto a 120-mg/cm^2 thick Bi backing plus a 132-mg/cm^2 thick Cu layer for heat dissipation. Approximately 95% of the reaction products were stable nuclei, stopped inside the Bi backing. The pulsing system was placed at the injection line of the FN Tandem accelerator and comprises five deflectors aligned parallel to the beam axis. The electric potential of one side of the deflectors was grounded, while the electrical potential of the opposite side was alternating between ground level and 1.3 kV.

The first pulsed beam had a pulse width of 75 ms and a repetition rate of 3.33 Hz. To exclude the background from β-decay channels and longer-lived isomers, a second pulsed beam was employed with a pulse width of 3.75 s and a repetition rate of 66.66 mHz. γ rays were measured using the HORUS array [31] comprising 14 HPGe detectors, six of them equipped with BGO Compton-suppression shields. The detectors were positioned on the eight corners and six faces of a cube. γ events were processed triggerless and recorded utilizing the synchronized 80-MHz XIA^{TM} Digital Gamma Finder (DGF) data-acquisition system. In addition, a reference signal given by the pulsing system was recorded.

The data were sorted into (i) a two-dimensional γ-γ matrix with a time gate of 250 ns between coincident γ events, (ii) a two-dimensional γ-t matrix to gate on different time windows relative to the reference pulse, and (iii) a total of three group matrices each corresponding to detector pairs with relative angles $\Theta = \{54.7^\circ, 70.4^\circ, 90^\circ\}$ for off-beam angular-correlation measurements using the SOCO-V2 code [38]. In total, 7.1×10^7 $\gamma\gamma$-coincidence events and 1.2×10^9 γ-t events were collected.

Spins and parities of populated states in the HORUS experiment are investigated in the off-beam measurement with the $\gamma\gamma$ angular-correlation code CORLEONE [39,40] based on the phase convention by Krane, Steffen, and Wheeler [41,42]. Different hypotheses of involved spins J_1, J_2, J_3 and multipole-mixing ratios δ_1, δ_2 of two coincident γ rays in a cascade $J_1 \xrightarrow{\delta_1} J_2 \xrightarrow{\delta_2} J_3$ are evaluated by χ^2 fits of the correlation function $W(J_1, \delta_1, J_2, \delta_2, J_3, \Theta, \sigma)$ to experimental correlation intensities for the three angular-correlation groups. θ_1 and θ_2 are the angles between beam axis and detectors; $\Theta = \theta_1 - \theta_2$ denotes the relative angle of a detector pair. A deorientation from the beam axis is taken into account by increasing the value of σ.

III. RESULTS

Partial level schemes of excited states in ^{133}Xe and ^{135}Ba, which are discussed in this paper, are displayed in Figs. 2(a) and 2(b). The determined half-lives of isomeric states in ^{132,133}Xe and ^{135,136}Ba are summarized in Table I.

The Doppler-corrected beamlike singles γ-ray spectrum gated on ^{135}Ba from the ^{136}Xe + ^{208}Pb AGATA experiment is shown in Fig. 3(a). Random background is significantly suppressed by gating on the prompt peak in the time-difference distribution between AGATA and PRISMA. Prominent transitions are marked with labels. The decays of the $J^\pi = 19/2^-_1$ and $15/2^-_1$ states at energies of 1052 and 682 keV are clearly visible as dominant peaks in the spectrum. Transitions in the positive-parity dipole band, on top of the $J^\pi = 21/2^+_2$ state at $E_x = 3083$ keV are observed well above the background. The highest excitation energy identified in the ^{135}Ba reaction channel corresponds to the $J^\pi = 31/2^+$ state at $E_x = 4696$ keV. The insets Figs. 3(b) and 3(c) show magnifications into the measured γ-ray spectrum around the γ-ray energies of the expected decays of the $J^\pi = 23/2^+$ state at 254 keV and around the decay of the $J^\pi = 19/2^-_2$ state at 1184 keV, respectively. The 1184-keV transition is clearly visible in the prompt AGATA spectrum, however, the 254-keV feeding transition is absent. This observation suggests that the half-life of the 2388-keV state is significantly longer compared to the width of the prompt peak in the time-difference spectrum between PRISMA and AGATA, i.e., $\Delta t_{\text{PRISMA}-\text{AGATA}} \approx 16$ ns. Consequently, the observation of the 1184-keV transition accompanied by the absence of the 254 keV feeding transition, despite the observation of other high-spin bands, indicates an isomeric character of the $E_x = 2388$ keV state.

In the first part of the HORUS experiment, the beam pulse width was set to 75 ms, followed by a 225-ms time window for off-beam measurements. The recorded reference time at the beginning of the beam flash allows us to gate on different off- and in-beam time windows. In particular, gates within the time window between 75 and 300 ms with respect to the reference pulse restrict the γ-ray spectrum to the off-beam measurement. Figures 3(d) and 3(f) show γ-ray spectra obtained with different time windows. The γ-time matrices with the applied gates are shown in inset Figs. 3(e) and 3(g). In the matrix a distinct separation between in-beam and off-beam γ-ray spectrum is visible at 75 ms relative to the reference pulse.

In order to validate the experimental procedure, several well-known long-lived millisecond isomers were investigated. By gating on the time window $\Delta t = 80$–90 ms [Fig. 3(d)], delayed transitions at energies of 174, 538, 600, 668, and 773 keV, forming a cascade below the $J^\pi = 10^+_1$ isomer in ^{132}Xe, are clearly enhanced in the γ-ray spectrum. Furthermore, the spectrum exhibits the 1048-keV $4^+_1 \rightarrow 2^+_1$ and 819-keV $2^+_1 \rightarrow 0^+_1$ transitions originating from the $J^\pi = 7^-_1$ isomer in ^{136}Ba. The peaks at 231, 948, and 695 keV are mutually coincident and identified as the decay cascade of the $J^\pi = 23/2^+_1$ state in ^{133}Xe. A background-subtracted

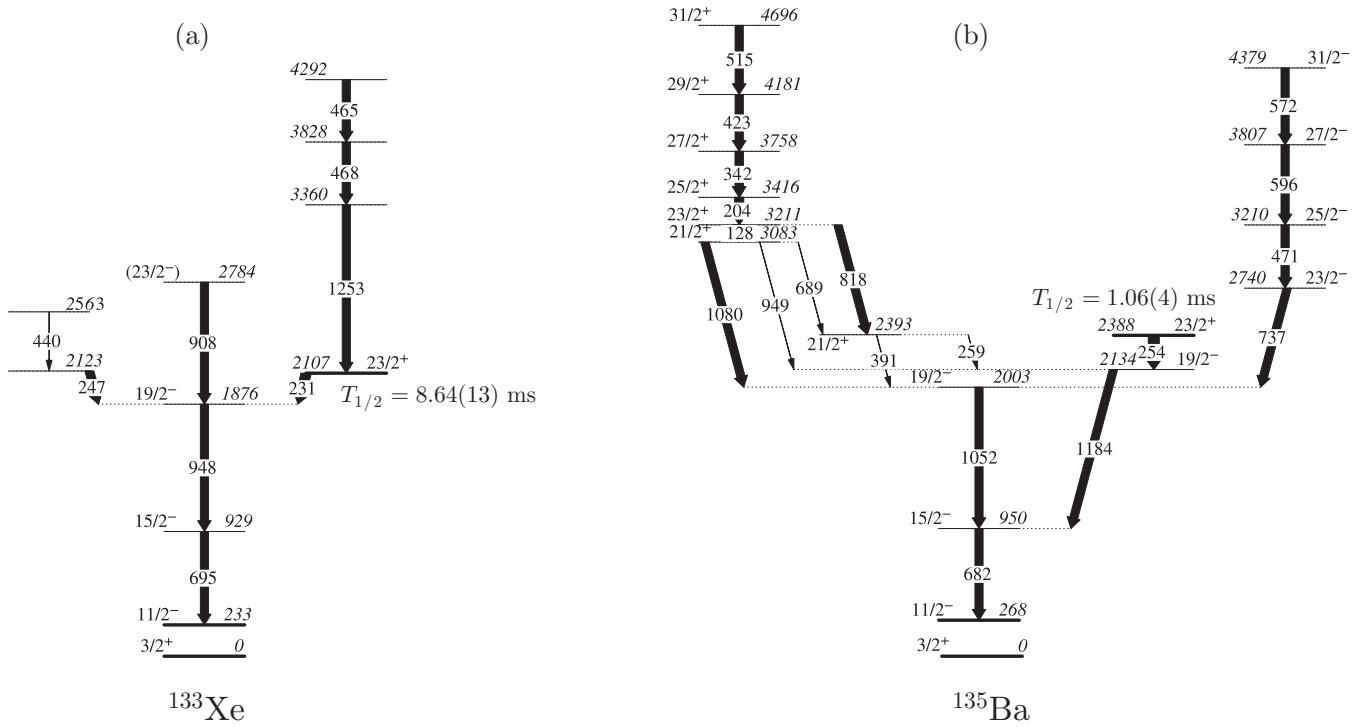

FIG. 2. Partial level schemes of (a) ^{133}Xe and (b) ^{135}Ba. The reduced transition strengths of the 231-keV transition in ^{133}Xe and the 254-keV transition in ^{135}Ba are subject of this paper. Dominating transitions in the HORUS fusion-evaporation experiment are presented with thicker arrows.

in-beam prompt $\gamma\gamma$-coincidence spectrum with a gate on the 1253-keV transition in ^{133}Xe is shown in Fig. 4. Coincident transitions at energies of 465 and 468 keV are forming a 1253-468-465 keV cascade on top of the $J^\pi = 23/2^+$ isomer confirming the observation in Ref. [5]. Other lines at 197, 847, 1039, and 1239 keV originate from the ^{19}F$(n, n'\gamma)$ reactions and the β decay of ^{56}Mn into ^{56}Fe.

The delayed transitions in ^{132,133}Xe and ^{136}Ba are also visible in the spectrum gated on the time window $\Delta t = 75$-80 ms in Fig. 3(f). Based on the AGATA data set, a pronounced delayed 254-1184-682-keV γ-ray cascade in ^{135}Ba is expected. The observation of this cascade in the off-beam spectrum in Fig. 3(f) clearly confirms the presence of an isomer in this nucleus. The absence of the cascade in the spectrum in Fig. 3(d) implies that the isomer in ^{133}Xe has a longer half-life compared to the similar state in ^{135}Ba.

Figures 5(a$_{1,2}$)–5(c$_{1,2}$) show fits of well-known half-lives of isomeric states in ^{136}Ba and ^{132}Xe. The fit function of the time spectrum $N(t)$ is chosen as $N(t) = a\exp[t\ln(2)/T_{1/2}] + b$ with a and b as free parameters. The decay chain deexciting the $J^\pi = 7^-$ isomer in ^{136}Ba is observed in the seconds-range pulsed-beam experiment. The corresponding background-subtracted time projection of the $2_1^+ \to 0_1^+$ transition at $E_\gamma = 819$ keV and the fitted decay

TABLE I. Measured half-lives of selected isomers observed in the ^{9}Be + ^{130}Te experiment. The different columns indicate the nucleus, repetition rate of the pulsed beam, excitation energy, spin and parity of the isomeric state, the energy of the γ ray used to determine the half-life, the deduced weighted mean half-life, and previous results reported in the literature.

Isotope	Repetition rate (Hz)	E_i (keV)	J_i^π ($\hbar$)	E_γ (keV)	$T_{1/2}$	
					Present work	Literature
^{136}Ba	0.066	2031	7^-	819	0.296(7) s	0.3084(19) s [43]
						0.303(2) s [44]
						0.37(5) s [45]
						0.32(2) s [46]
^{132}Xe	3.33	2752	10^+	174, 538, 600, 668, and 773	8.37(8) ms	8.39(11) ms [47]
						8.4(8) ms [48]
						8.2(6) ms [49,50]
^{133}Xe	3.33	2107	$23/2^+$	231, 695, and 948	8.64(13) ms	–
^{135}Ba	3.33	2388	$23/2^+$	254, 682, and 1184	1.06(4) ms	–

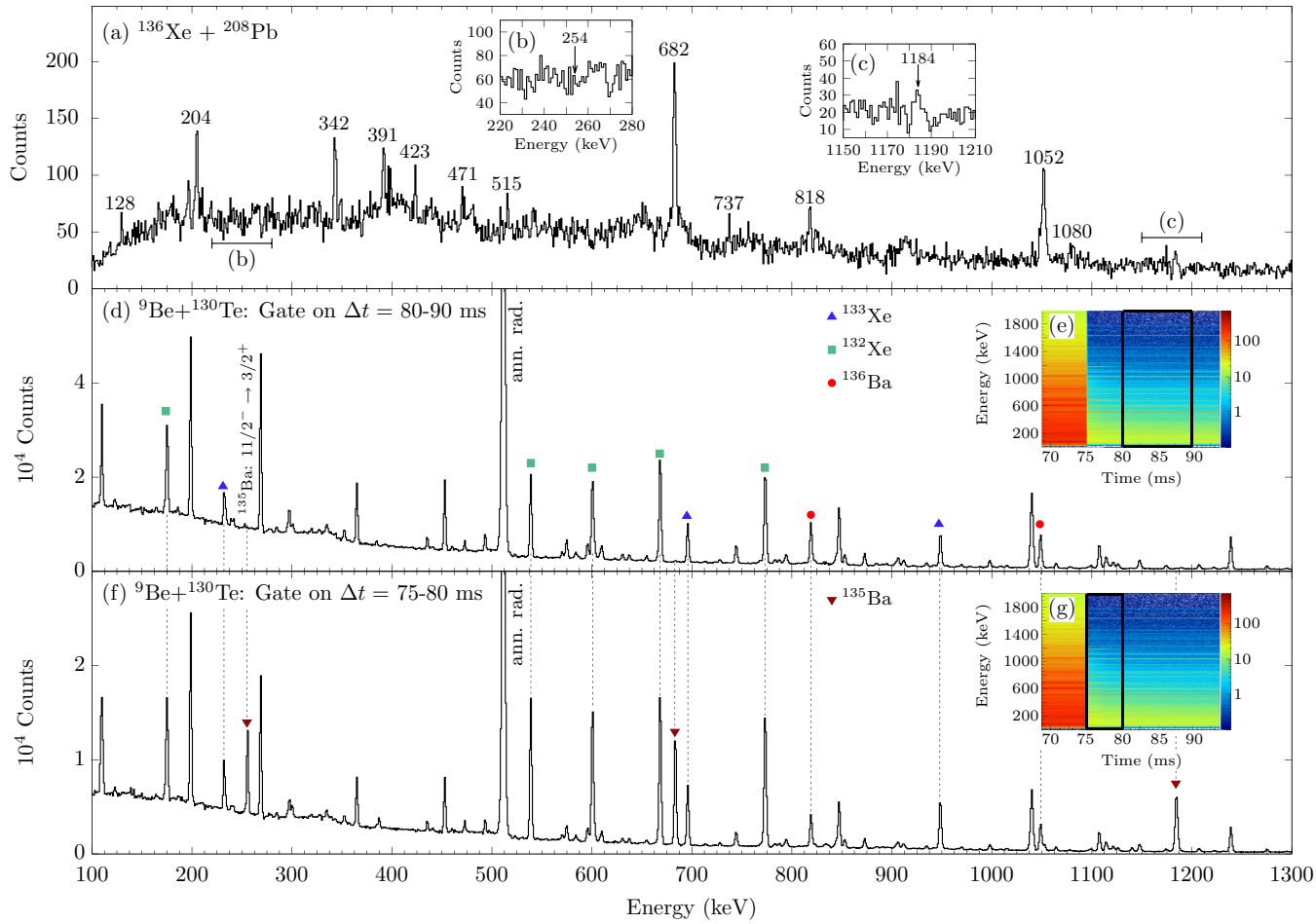

FIG. 3. (a) Doppler-corrected γ-ray spectrum gated on ^{135}Ba identified with PRISMA in the ^{136}Xe+^{208}Pb experiment. Insets show the zoomed spectrum around the expected transitions at (b) 254-keV and (c) 1184-keV. (d) Projection of the γ-t matrix gated on a time window between 80 and 90 ms relative to the reference time at the beginning of the beam flash. (f) Similar data for a gate on a time window between 75 and 80 ms. Delayed transitions below the $J^\pi = 23/2^+_1$ isomers in ^{133}Xe, ^{135}Ba, and below the $J^\pi = 10^+_1$ isomer in ^{132}Xe are marked with symbols and dashed lines to guide the eye. Both insets (e) and (g) present the γ-t matrix relative to the reference time. The applied time gates are surrounded by black boxes.

curve are shown in Fig. 5(a_1). For the sake of completeness, a similar plot with a logarithmic scale is shown in the inset Fig. 5(a_2). The measured half-life of $T_{1/2} = 0.296(7)$ s is in good agreement with previously measured values [44–46]. The absolute fit residual, defined as difference between absolute experimental value and fit function, is presented in Fig. 5(a_3). In addition, fits of the background-subtracted time projections of the 538-keV and 668-keV transitions, depopulating the $J^\pi = 10^+$ isomer in ^{132}Xe, are depicted in Fig. 5($b_{1,2}$) and Fig. 5($c_{1,2}$). A small constant background remains after background subtraction in the time distribution of the $2^+_1 \rightarrow 0^+_1$ 668 keV transition due to a weak feeding from β decays of ^{132}I and ^{132}Cs. Both independently determined half-lives are in excellent agreement with the previous values [47–50]. The consistency between the literature values and the current analysis demonstrates the reliability of the analysis.

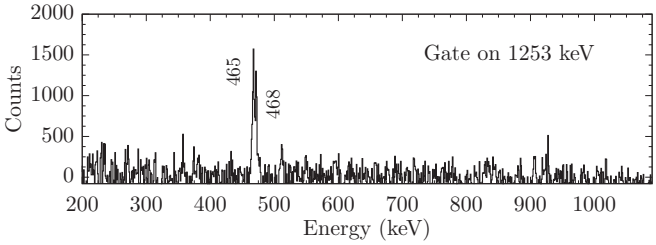

FIG. 4. Prompt in-beam $\gamma\gamma$ coincidence spectrum with a gate on the 1253-keV transition in ^{133}Xe above the $J^\pi = 23/2^+$ isomer. Coincidences at energies of 465 and 468 keV are visible.

The background-subtracted time distributions of the 231-, 947-, and 695-keV transitions in ^{133}Xe are presented in Figs. 5($c_{1,2}$), 5($d_{1,2}$), and 5($e_{1,2}$). Exponential fits of the slope components yield respective half-lives of 8.62(13), 8.60(9), and 8.68(8) ms. The constant random background is determined separately and incorporated into the fit. The independently determined half-lives utilizing the three different gate conditions show excellent agreement. Systematic errors from uncertainties in the determination of the background

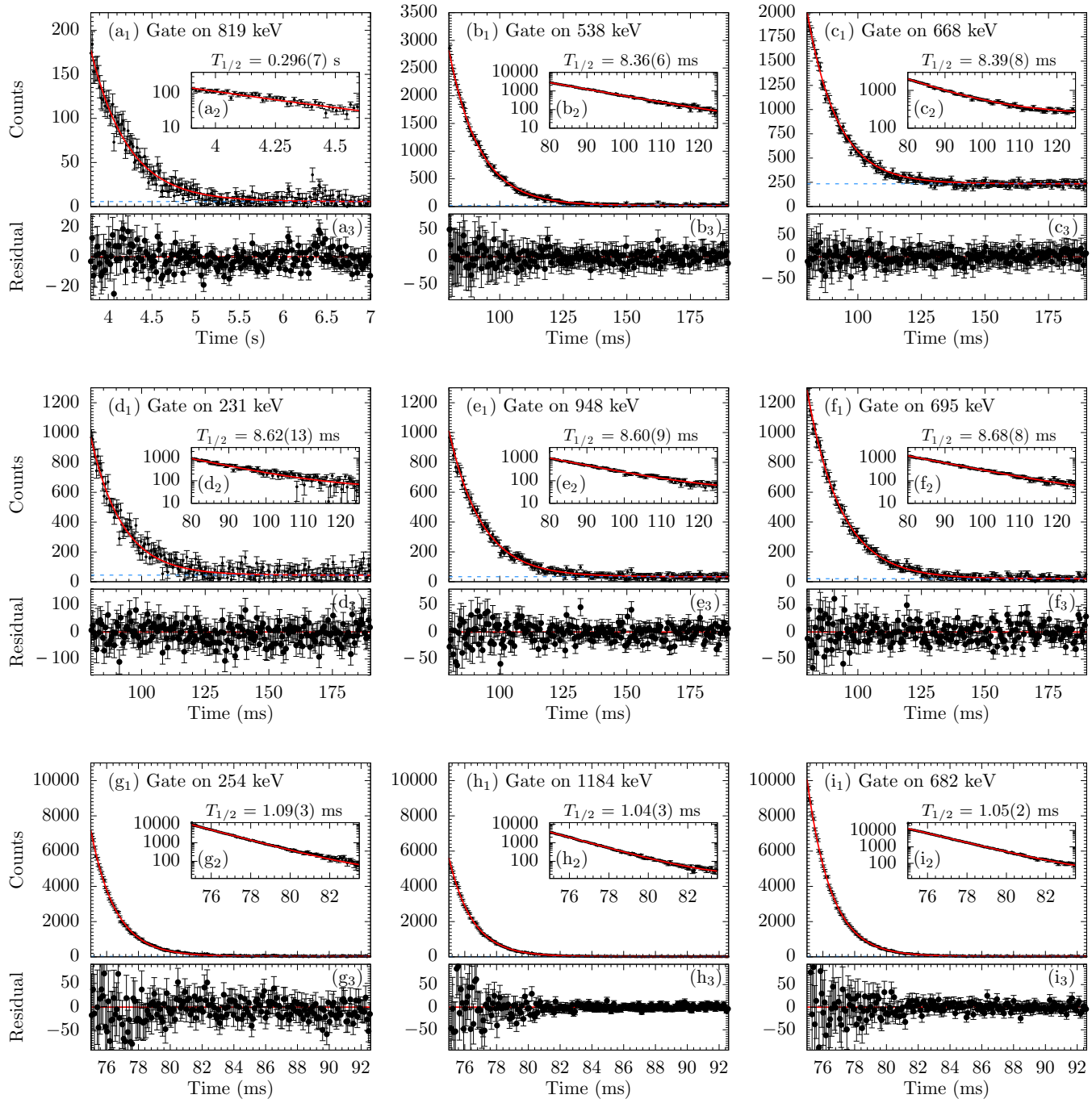

FIG. 5. Gates on background-subtracted γ-time matrices and half-life fits for the gating conditions ($a_{1\text{-}2}$) 819 keV in ^{136}Ba measured in the seconds-pulsing experiment, ($b_{1\text{-}2}$) 538 keV and ($c_{1\text{-}2}$) 668 keV in ^{132}Xe, ($d_{1\text{-}2}$) 231 keV, ($e_{1\text{-}2}$) 947 keV, and ($f_{1\text{-}2}$) 695 keV in ^{133}Xe, ($g_{1\text{-}2}$) 254 keV, ($h_{1\text{-}2}$) 1184 keV, and ($i_{1\text{-}2}$) 682 keV in ^{135}Ba obtained in the milliseconds-pulsing experiment. The corresponding residual, defined as difference between absolute value and fit function, is shown in panels (a_3), (b_3), (c_3), (d_3), (e_3), (f_3), (g_3), (h_3), and (i_3), respectively. Half-lives are determined from exponential fits of the delayed component. The fit is drawn with a solid red line. Random background is determined separately (dashed blue line) and incorporated into the fit model.

are taken into account. The final weighted mean value of $T_{1/2} = 8.64(13)$ ms is newly established for the $J^\pi = 23/2^+$ state in ^{133}Xe.

Background subtracted time spectra of transitions deexciting the state at $E_x = 2388$ keV in ^{135}Ba, fits, and corresponding residuals are presented in Figs. 5(f_1)–5(h_3). The fit for the 254-keV transition yields a half-life of 1.09(3) ms. Independently determined half-lives involving the 1184-keV [1.04(3) ms], and the 682-keV [1.05(2) ms] γ ray are in mutual agreement. The final weighted mean half-life of the $J^\pi = 23/2^+$ state in ^{135}Ba is measured to be $T_{1/2} = 1.06(4)$ ms taking into account systematic errors.

According to systematics and shell-model arguments, a direct single-step decay of the $2107 + x$-keV band head of the 465-468-1253-keV cascade in ^{133}Xe via a 231-keV transition was slightly favored in the previous work [5]. However, a decay via an unobserved low-energy transition similar to ^{129}Sn and ^{139}Nd could not be ruled out. Internal conversion coefficients and angular-correlation measurements were carried out to clarify the decay patterns in ^{133}Xe and ^{135}Ba. Since conversion electrons are not directly detected, the internal conversion coefficient α_T is determined via the intensity-balance method described in Ref. [52]. In the off-beam measurement the isomer in ^{133}Xe decays via the 231-948-695 cascade towards the $J^\pi = 11/2^-$ state. Therefore, the intensities of the 231 and 948-keV transitions, corrected for detector efficiency and internal conversion, are equal in the delayed γ-ray spectrum:

$$I_{\gamma_1}(1 + \alpha_{\gamma_1}) = I_{\gamma_2}(1 + \alpha_{\gamma_2}), \tag{1}$$

where $I_{\gamma_{1,2}}$ are the efficiency-corrected γ-ray intensities and $\alpha_{\gamma_{1,2}}$ are the total internal-conversion coefficients (ICCs). The off-beam intensities $I_{948\ \mathrm{keV}}$ and $I_{231\ \mathrm{keV}}$ are extracted from the γ-ray spectra of the 14 HPGe detectors by gating on the off-beam time window with a time gap of 100 ns from the in-beam part to exclude possible feeding from short-lived components. Using the weighted arithmetic mean of the 14 measurements and the well-established $E2$ character of the 948 keV transition ($\alpha_{948} = 0.00182$ [51]), a value of $\alpha_{231} = 0.49(9)$ is obtained for the 231-keV transition. Based on a comparison with theoretical α_T values [51], presented in Fig. 6(a), the multipolarity of the 231-keV transition can be restricted to an $M2$ or $E3$ character. Applying the same method to the 254-1184-keV cascade in ^{135}Ba, a value of $\alpha_{254} = 0.32(7)$ for the 254 keV transition is computed. Again, a comparison with theoretical values shown in Fig. 6(b) yields a good agreement with $M2$ or $E3$ multipolarities for the 254-keV γ ray.

Angular-correlation measurements provide a complementary approach to the internal conversion coefficient measurement. Figures 6(c)–6(e) show comparisons of theoretical angular-correlation functions $W(J_1, \delta_1, J_2, \delta_2, J_3, \Theta, \sigma)$ (colored lines) with experimentally obtained relative intensities in three different correlation groups. A fit of the $2_2^+ \rightarrow 2_1^+$ 1120-keV transition in ^{214}Po, measured in the energy calibration run with a ^{226}Ra source, is shown in Fig. 6(c). The determined multipole-mixing ratio of $\delta = 0.19(6)$ agrees well with the evaluated multipole-mixing ratio of $\delta_{\mathrm{lit.}} = 0.18(2)$ [53]. The corresponding angular-correlation fit of the 231-keV transition, gated on the 948-keV transition in ^{133}Xe, is presented in Fig. 6(d). The multipolarity of the 948-keV γ ray is fixed to be an $E2$ transition, while different spin hypotheses of the 2107-keV state are tested. Combined with the internal conversion coefficient measurement, a spin assignment of $J^\pi = 23/2^+$ and a multipole-mixing ratio of $\delta_{23/2^+ \rightarrow 19/2^-} = -0.021(10)$ is most likely for the 2107-keV state. The small value of the multipole-mixing ratio indicates a dominant $M2$ contribution and a small $E3$ admixture in the $\Delta J = 2$ transition.

Spin hypotheses for the 2388-keV state in ^{135}Ba are tested by employing the same angular-correlation method. In Fig. 6(e) experimentally determined intensities of the 254-keV γ ray in the different correlation groups, gated on the 1184-keV transition, are compared to theoretical intensities.

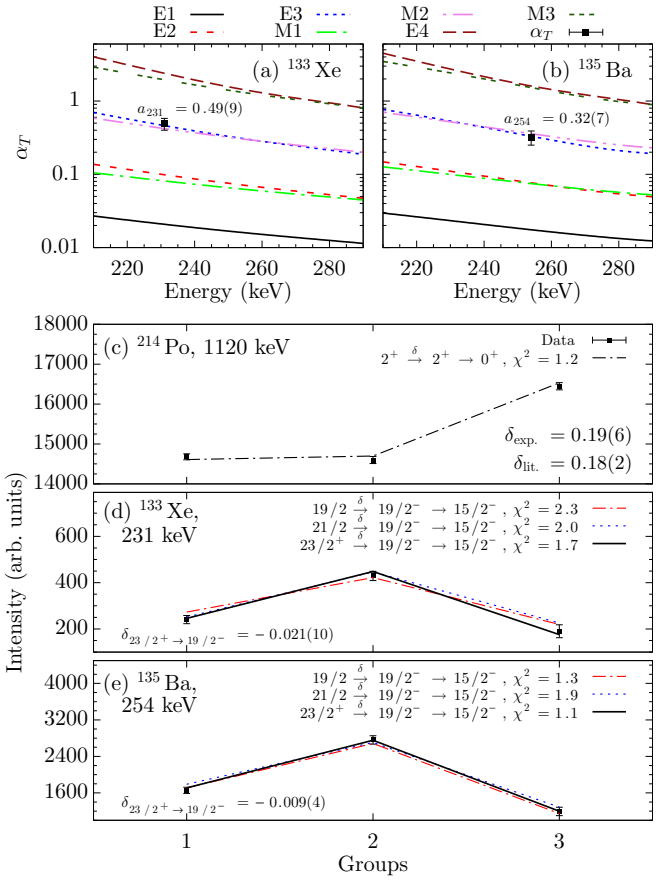

FIG. 6. (a) Total conversion coefficient for the 231-keV transition in ^{133}Xe compared with predicted values from the BrIcc v2.3 database [51]. (b) Similar comparison for the 254-keV transition in ^{135}Ba. The multipolarity of the 231 and 254-keV transition can be restricted to $M2/E3$ character. $\gamma\gamma$ off-beam angular correlations for (c) the known 1120-609-keV cascade in ^{214}Po, (d) the 231-948-keV cascade in ^{133}Xe, and (e) the 254-1184-keV cascade in ^{135}Ba. Experimental values (black points) are compared to calculated angular-correlation functions $W(J_1, \delta_1, J_2, \delta_2, J_3, \Theta, \sigma)$ (lines) for three correlation groups.

Again, the $23/2^+ \xrightarrow{\delta} 19/2^- \rightarrow 15/2^-$ hypothesis (solid line) with $\delta_{23/2^+ \rightarrow 19/2^-} = -0.009(4)$ yields the best agreement. The small multipole-mixing ratio indicates a dominating $M2$ character of the 254-keV transition. Nevertheless, based on the fit results of this work, a spin assignment of $J = 19/2$ ($\chi^2 = 1.9$) or $21/2$ ($\chi^2 = 1.3$) cannot be excluded either. However, the internal conversion coefficient measurement shown in Fig. 6(b) suggests a $J^\pi = 23/2^+$ spin assignment. This argument is further supported by the previous results of Ref. [26], where both spin assignments $J = 19/2$ and $J = 21/2$ are excluded.

Internal-conversion coefficients are calculated employing the newly determined multiple-mixing ratios δ via the following expression [54]:

$$\alpha_T = \frac{\alpha_T(M2) + \delta^2 \alpha_T(E3)}{1 + \delta^2}, \tag{2}$$

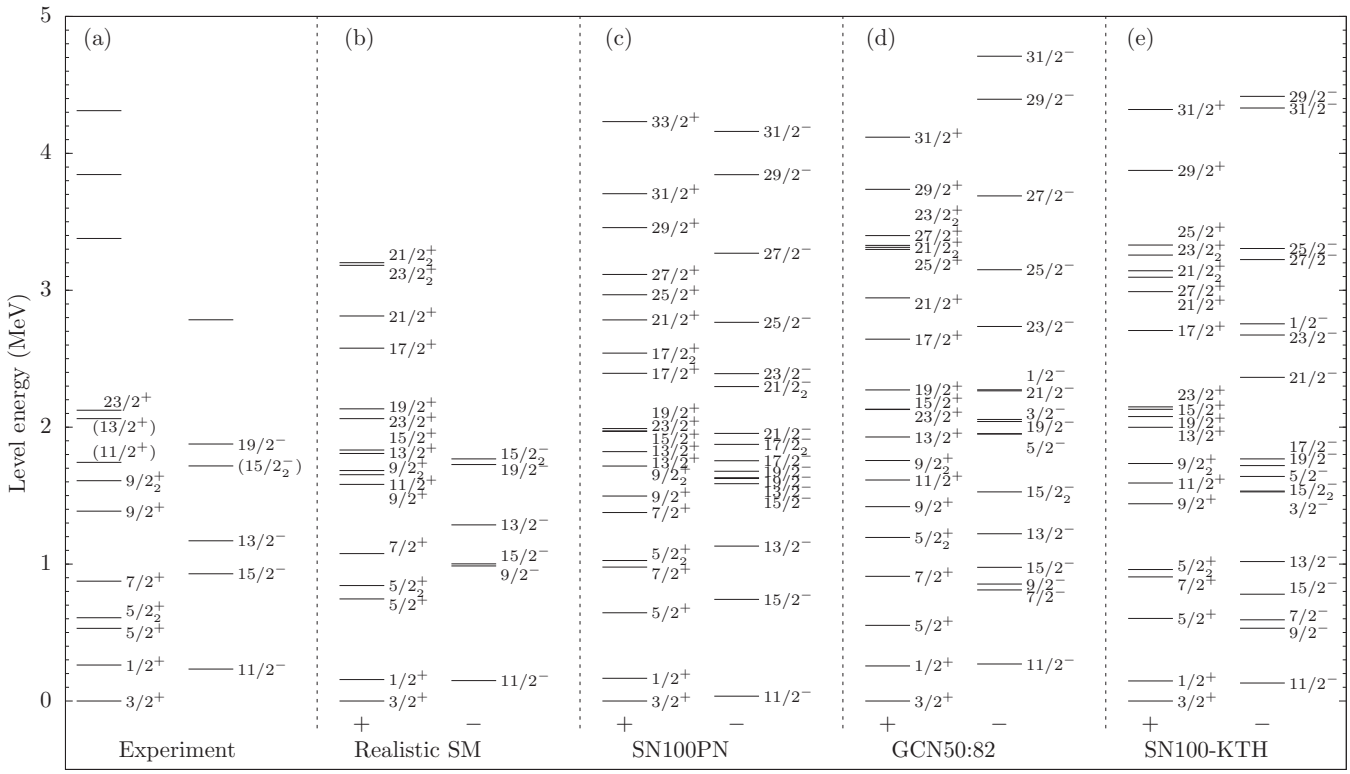

FIG. 7. Comparison of experimental energy spectra of ^{133}Xe [left panel, (a)] with the results of shell-model calculations employing the (b) Realistic SM, (c) SN100PN, (d) GCN50:82, and (e) SN100-KTH interaction. Note that the states are separated into columns for the negative- and the positive-parity states.

where $\alpha_T(M2)$ and $\alpha_T(E3)$ are theoretical ICC values. The calculated values $\alpha_T = 0.421(6)$ for ^{133}Xe and $\alpha_T = 0.364(5)$ for ^{135}Ba are in good agreement with the independently measured ICC values, showing the complementarity between both approaches.

IV. DISCUSSION

The experimentally obtained isomer excitation energies, half-lives and corresponding reduced transition probabilities in ^{133}Xe and ^{135}Ba are compared to shell-model theory. All shell-model calculations were carried out in an untruncated *gdsh* valence space outside doubly magic ^{100}Sn, employing the shell-model code NUSHELLX@MSU [55], the massive-parallelization code KSHELL [56] and the ANTOINE shell-model code [57].

The first calculation is conducted in the framework of the realistic shell model [58,59], denoted as realistic SM. Single-particle energies and two-body effective interaction are determined from the established CD-Bonn free nucleon-nucleon potential using the $V_{\text{low-}k}$ approach with a cutoff momentum of $\Lambda = 2.6$ fm^{-1}, plus the Coulomb force for protons. The effective shell-model Hamiltonian is derived iteratively by means of the many-body perturbation theory in the $\hat{Q}$-box folded diagram expansion, including all diagrams up to third order in the interaction.

Another calculation is carried out with the jj55pn Hamiltonian (referred to as the SN100PN interaction) [60]. The Hamiltonian consists of four terms covering the neutron-neutron, neutron-proton, proton-proton, and Coulomb repulsion between the protons individually. A renormalized G matrix derived from the CD-Bonn interaction [61] was employed to construct the realistic two-body residual interaction. The proton and neutron single-particle energies are based upon the energy levels in ^{133}Sb and ^{131}Sn.

A third calculation is performed utilizing the effective interaction GCN50:82 [62,63]. Similar to the SN100PN interaction, the interaction is derived from a realistic G matrix based on the CD-Bonn potential. Empirical monopole corrections to the original G matrix are introduced by fitting different combinations of two-body matrix elements to sets of experimental excitation energies from even-even and even-odd semimagic nuclei.

The last calculation, hereinafter referred to as SN100-KTH, leverages the realistic CD-Bonn interaction as well. The $T = 1$ part of the monopole interaction was corrected via the Monte Carlo global optimization approach by fitting several low-lying yrast states in Sn isotopes. A renormalization was performed by a perturbative G matrix approach to include core-polarization effects. It was shown that the calculations reproduce well the excitation energies and $E2$ transition probabilities in even-even Te isotopes [64,65].

A comparison of [Fig. 7(a)] experimental energy spectrum of ^{133}Xe with the results of [Fig. 7(b)] realistic SM, [Fig. 7(c)] SN100PN, [Fig. 7(d)] GCN50:82, and [Fig. 7(e)] SN100-KTH shell-model calculations is shown in Fig. 7. The states are separated into columns for the negative- and the positive-parity states. All four calculations reproduce the spin

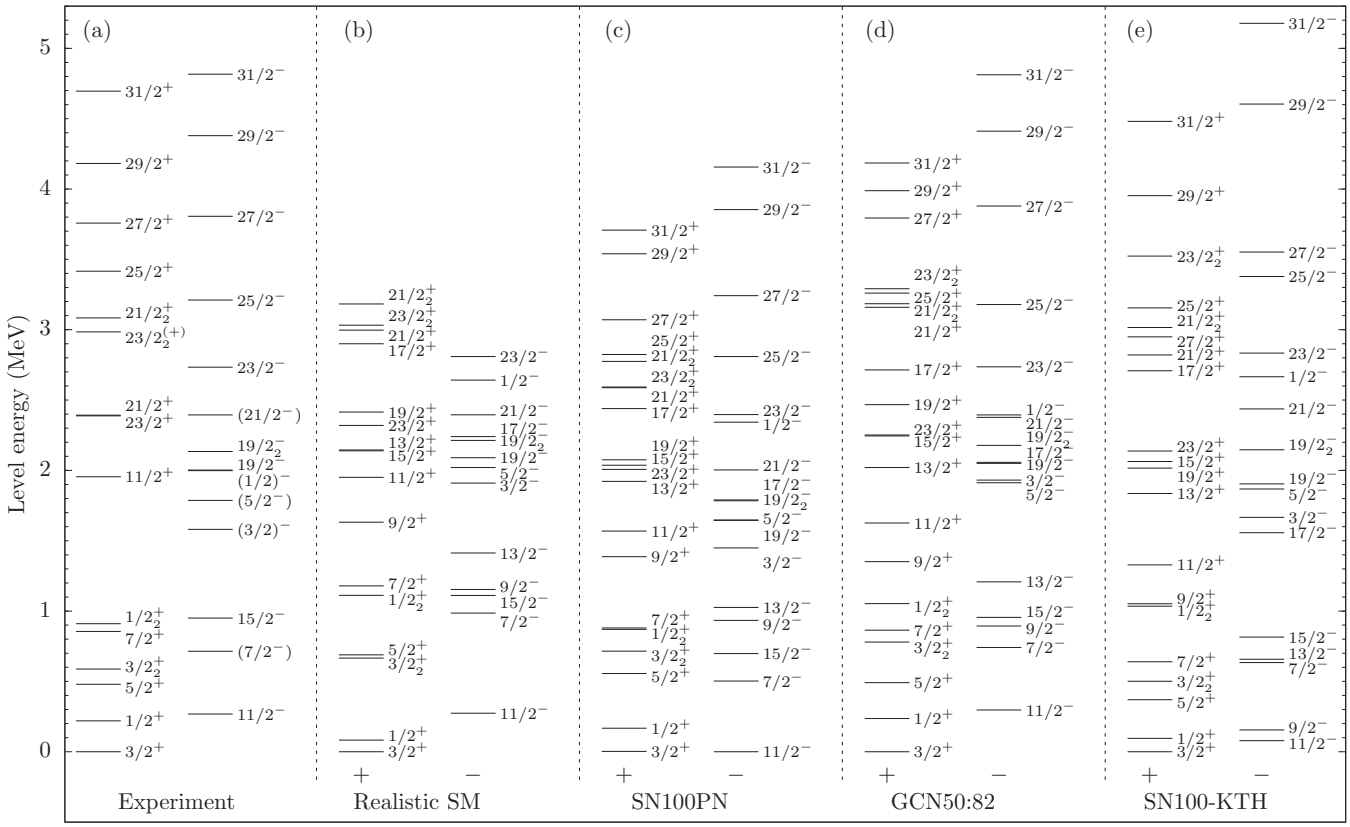

FIG. 8. Comparison of experimental energy spectra of ^{135}Ba [left panel, (a)] with the results of shell-model calculations employing the (b) Realistic SM, (c) SN100PN, (d) GCN50:82, and (e) SN100-KTH interactions. The arrangement of the states mirrors the layout in Fig. 7.

of the $J^\pi = 3/2^+$ ground state. The GCN50:82 interaction slightly overpredicts the $E_x = 233$-keV $J^\pi = 11/2_1^-$ state by 37 keV while the realistic SM, SN100PN, and SN100-KTH interactions place the $J^\pi = 11/2_1^-$ state 84, 198, and 102 keV too low in excitation energy, respectively. All interactions show a good agreement for the low-spin positive-parity states below 1 MeV.

The 948-, and 695-keV γ-ray transitions, forming the $19/2_1^- \to 15/2_1^- \to 11/2_1^-$ cascade, are calculated as 726 and 852 keV using realistic SM, 883 and 707 keV using SN100PN, 977 and 706 keV using GCN50:82, and as 939 and 649 keV using SN100-KTH, respectively. The calculated excitation energy of the isomeric $J^\pi = 23/2_1^+$ state is in excellent agreement with the experimental value exhibiting deviations of only 45 (realistic SM), 134 (SN100PN), 5 (GCN50:82), and 24 keV (SN100-KTH). Additionally, the $23/2_1^+ \to 19/2_1^-$ transition is computed as $E_\gamma =$ 335 keV (realistic SM), $E_\gamma = 348$ keV (SN100PN), $E_\gamma =$ 176 keV (GCN50:82), and $E_\gamma = 429$ keV (SN100-KTH), compared to the observed 231-keV γ-ray transition in the experiment.

The level structure of the $+2p$ isotone ^{135}Ba is more intricate. A comparison of [Fig. 8(a)] experimental energy spectra of ^{135}Ba with the shell-model results of [Fig. 8(b)] realistic SM, [Fig. 8(c)] SN100PN, [Fig. 8(d)] GCN50:82, and [Fig. 8(e)] SN100-KTH calculations are presented in Fig. 8. Again, the states are separated into columns for negative- and positive-parity states. The $J^\pi = 3/2_1^+$ ground state is well reproduced by the realistic SM, GCN50:82 and SN100-KTH interactions. However, the SN100PN interaction locates the $J^\pi = 3/2_1^+$ state 3 keV above the $J^\pi = 11/2_1^-$ state. The other three interactions compute the $J^\pi = 11/2_1^-$ state ($E_x =$ 268 keV) to have excitation energies of 274 (realistic SM), 297 (GCN50:82), and 79 keV (SN100-KTH). The interactions yield a good reproduction of the experimentally determined positive low-spin regime below 1 MeV excitation energy.

The interactions reproduce the $19/2_1^- \to 15/2_1^- \to 11/2_1^-$ cascade with γ-ray energies of 1052 and 682 keV very well. Deviations amount to 73 and 155 keV (Realistic SM), 105 and 16 keV (SN100PN), 43 and 26 keV (GCN50:82), as well as 37 and 54 keV (SN100-KTH). In the experiment the energy difference between the first and second excited $J^\pi = 19/2^-$ states is 131 keV, compared to the calculations of 123 (realistic SM), 139 (SN100PN), 128 (GCN50:82), and 243 keV (SN100-KTH). The calculated excitation energies for the first and second excited $J^\pi = 23/2^+$ states of 2320/3032 (realistic SM), 2007/2668 (SN100PN), 2252/3260 (GCN50:82), and 2138/3523 keV (SN100-KTH) are in good agreement with the experimentally determined $E_x = 2388/2985$ keV. Additionally, the $23/2_1^+ \to 19/2_2^-$ transition is computed as $E_\gamma = 126$ keV (realistic SM), $E_\gamma = 223$ keV (SN100PN), and $E_\gamma = 74$ keV (GCN50:82), compared to the observed 254-keV γ-ray transition in the experiment. Nonetheless, the SN100-KTH interaction is the only interaction, which computes the $J^\pi = 19/2_2^-$ state slightly above the $J^\pi = 23/2_1^+$ state.

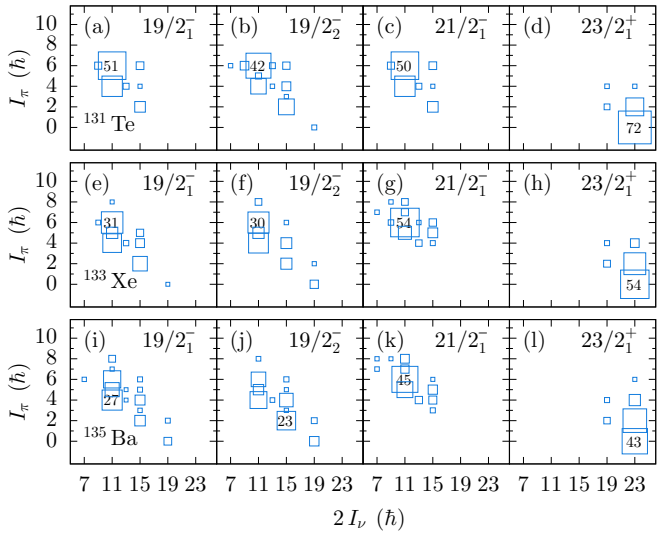

FIG. 9. Decomposition of the total angular momentum $I = I_\pi \otimes I_\nu$ into its proton and neutron components for the $J^\pi = 19/2_1^-$, $19/2_2^-$, $21/2_1^-$, and $23/2_1^-$ states in (a)–(d) ^{131}Te, (e)–(h) ^{133}Xe, and (i)–(l) ^{135}Ba calculated with the GCN50:82 interaction. Strongest components are labeled with corresponding percentages.

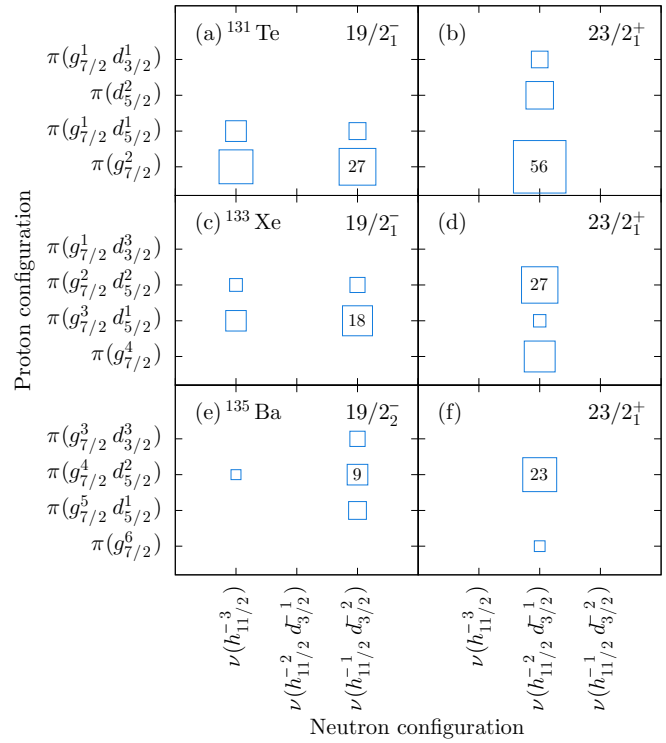

FIG. 10. Decomposition of the $J^\pi = 19/2^-$ and $23/2^+$ states of (a),(b) ^{131}Te, (c),(d) ^{133}Xe, and (e),(f) ^{135}Ba into their proton and neutron configurations computed by the GCN50:82 interaction. Strongest components are labeled with corresponding percentages.

The nuclear structures along the $N = 79$ isotones closely resemble each other. Figures 9(a)–9(l) show the decomposition of the total angular momentum $I = I_\pi \otimes I_\nu$ into its proton and neutron components for selected states using the GCN50:82 interaction. The decompositions are very similar to those computed by the SN100PN and SN100-KTH interactions. Although being more fragmented going from ^{131}Te to ^{135}Ba, the spin decompositions of the high-spin states above the $J^\pi = 11/2_1^-$ state are similar. In ^{131}Te and ^{133}Xe, the $J^\pi = 23/2_1^+$ state decays into the yrast $J^\pi = 19/2_1^-$ state, while in ^{135}Ba it decays into another yrare $J^\pi = 19/2^-$ state. Nevertheless, the spin decomposition of the first and second excited $J^\pi = 19/2^-$ states are almost identical.

The interaction predicts the $J^\pi = 23/2_1^+$ state to predominantly have (54% ^{133}Xe; 43% ^{135}Ba) $\nu\ 23/2^+ \otimes \pi\ 0^+$ and (32%; 37%) $\nu\ 23/2^+ \otimes \pi\ 2^+$ stretched neutron spin configurations. On the other hand, the $J^\pi = 19/2^-$ states in both ^{133}Xe and ^{135}Ba are mostly assigned to configurations with neutron spin $I_\nu = 11/2$ coupled to proton spins of $I_\pi = 4$ and $I_\pi = 6$. These configuration differences provide a microscopic reason of the long-lived $J^\pi = 23/2^+$ states; their decays require a considerable reordering of angular momentum for protons and neutrons, which strongly hinders a transition between both states.

The isomeric character is also scrutinized via a detailed decomposition of the $J^\pi = 19/2^-$, and $23/2^+$ states of the $N = 79$ isotones ^{131}Te, ^{133}Xe, and ^{135}Ba into their proton and neutron configurations computed by the GCN50:82 interaction, presented in Figs. 10(a)–10(f). The wave functions of the $J^\pi = 23/2_1^+$ states are dominated by the neutron $\nu(h_{11/2}^{-2} d_{3/2}^{-1})$ configuration with probabilities of 81.3% (^{131}Te), 60.3% (^{133}Xe), and 44.0% (^{135}Ba). Also the SN100PN and SN100-KTH calculations yield a dominant $\nu(h_{11/2}^{-2} d_{3/2}^{-1})$ neutron configuration.

In contrary, with GCN50:82, the leading neutron configurations of the final $J^\pi = 19/2^-$ state are $\nu h_{11/2}^{-3}$ and $\nu(h_{11/2}^{-1} d_{3/2}^{-2})$ contributing with probabilities of 31.4% and 34.3% in ^{131}Te, 13.7% and 24.8% in ^{133}Xe, as well as 4.9% and 20.3% in ^{135}Ba. The $\nu(h_{11/2}^{-2} d_{3/2}^{-1})$ configuration nearly vanishes in the decomposition of the $J^\pi = 19/2^-$ states. The dominant components of the $J^\pi = 19/2^-$ and $23/2^+$ states can be connected by a $M2$ transition operator, however, the hindrance of the $M2$ transition can be traced back mainly due to the change of the neutron content of the states.

Finally, reduced transition probabilities for the $23/2^+ \to 19/2^-$ transitions in ^{131}Te, ^{133}Xe and ^{135}Ba are calculated with the realistic SM, SN100PN, GCN50:82, and SN100-KTH interactions. Modified g factors of $g_l = g_{l_{\rm free}}$ and $g_s = 0.68 g_{s_{\rm free}}$ for protons and neutrons are used for the SN100PN, GCN50:82, and SN100-KTH interactions. The obtained quenching factor of 0.68 is tuned to reproduce the magnetic moments of the $J^\pi = 11/2_1^-$ states in ^{129}Sn ($\mu = -1.297(5)\mu_n$ [66]) and ^{131}Te ($\mu = -1.123(7)\mu_n$ [67]). In the realistic SM calculation nuclear g factors of $g_l = 1.2$, $g_s = 3.91$ for protons and $g_l = 0.2$, $g_s = -2.678$ for neutrons are employed.

The effective charges for protons and neutrons are selected to reproduce the $E2$ transition strengths of the first excited $J^\pi = 2^+$ state in the $Z = 50$ isotope ^{128}Sn ($B(E2; 2^+ \to 0^+) = 4.2(3)$ W.u. [68]) and of the $19/2^- \to 15/2^-$ decay ($B(E2; 19/2^- \to 15/2^-) = 2.56(14)$ W.u. [69]) in ^{133}Te using the SN100PN, GCN50:82, and SN100-KTH interactions.

TABLE II. Summary of experimental and theoretical results for $E2$, $M2$, and $E3$ reduced transition strengths of the $N = 79$ isotones ^{129}Sn, ^{131}Te, ^{133}Xe, and ^{135}Ba. Transition strengths are given in Weisskopf units. Experimental values of ^{129}Sn and ^{131}Te are taken from Refs. [1,4,6].

Isotope	$J_i^\pi \to J_f^\pi$	E_i (keV)	$T_{1/2}$ (ms)	$\sigma\lambda$	$B(\sigma\lambda)\downarrow$ (W.u.)				
					Experiment	Theory			
						Realistic SM	SN100PN	GCN50:82	SN100-KTH
^{129}Sn	$27/2_1^- \to 23/2_1^-$	2552	$0.27(7) \times 10^{-3}$	$E2$	0.79(36)	–	0.72	0.72	0.72
	$23/2_1^+ \to 19/2_1^+$	1802	$2.4(2) \times 10^{-3}$	$E2$	1.24(10)	–	1.45	0.71	1.44
	$19/2_1^+ \to 15/2_1^+$	1761	$3.6(2) \times 10^{-3}$	$E2$	1.37(8)	–	2.11	1.78	2.14
^{131}Te	$19/2_1^- \to 15/2_1^-$	1581	$71(20) \times 10^{-9}$	$E2$	3.5(10)	–	4.9	2.9	3.5
	$23/2_1^+ \to 19/2_1^-$	1941	93(12)	$M2$	$2.0(3) \times 10^{-6}$	–	404×10^{-6}	197×10^{-6}	305×10^{-6}
^{133}Xe	$23/2_1^+ \to 19/2_1^-$	2107	8.64(13)	$M2$	$0.209(3) \times 10^{-3}$	1.163×10^{-3}	1.613×10^{-3}	0.668×10^{-3}	1.691×10^{-3}
				$E3$	0.0017(16)	0.476	0.124	0.021	0.221
^{135}Ba	$23/2_1^+ \to 19/2_2^-$	2388	1.06(4)	$M2$	$1.053(40) \times 10^{-3}$	4.12×10^{-3}	2.440×10^{-3}	3.878×10^{-3}	2.283×10^{-3}
				$E3$	0.0012(11)	1.161	0.144	0.119	0.164

The adopted effective charges are $e_\nu = 0.81e$ and $e_\pi = 1.52e$. Selected values are in excellent agreement with the effective charges used in a recent study of the $N = 81$ isotonic chain [70] and the previous study of ^{136}Ba [71]. In the realistic SM calculation effective charges of $e_\nu = 0.7e$ and $e_\pi = 1.7e$ are used.

The newly established half-lives are converted into $M2$ and $E3$ reduced transition probabilities using the equations [72,73]:

$$B(M2) = \frac{5.12 \times 10^{-8}}{T_{1/2}E_\gamma^5} \frac{1}{1+\delta^2_{\frac{E3}{M2}}} \mu_N^2 \mathrm{fm}^2 \tag{3}$$

and

$$B(E3) = \frac{1.21 \times 10^{-3}}{T_{1/2}E_\gamma^7} \frac{\delta^2_{\frac{E3}{M2}}}{1+\delta^2_{\frac{E3}{M2}}} e^2 \mathrm{fm}^6, \tag{4}$$

where $T_{1/2}$, E_γ and $\delta_{\frac{E3}{M2}}$ correspond to the measured half-life of the initial state in seconds, the γ-ray energy in MeV and the multipole-mixing ratio of the γ ray. The experimentally deduced $B(\sigma\lambda)$ values and the results of the shell-model calculations are summarized in Table II.

To benchmark shell-model calculations, several previously known $B(E2)$ values of ^{129}Sn and ^{131}Te are added. The experimental $E2$ reduced transition strengths of the decay of the seniority $v = 3$ multiplet states $J^\pi = 19/2^+$, $23/2^+$, and $27/2^-$ [1,4] in ^{129}Sn are well described within the three shell-model calculations. The discrepancy between the three calculations stays below 50% for the $B(E2; 23/2^+ \to 19/2^+)$ value in ^{129}Sn. Moreover, the calculated $B(E2)$ transition probability of the $19/2^- \to 15/2^-$ decay in ^{131}Te agrees well with the experiment.

Assuming a pure $M2$ transition, the experimental $B(M2; 23/2^+ \to 19/2^-)$ value of the $E_\gamma = 360$-keV transition in ^{131}Te is $2.0(3) \times 10^{-6}$ W.u. [2]. This value is overpredicted by at least two orders of magnitudes by the shell-model calculations. The single-particle Weisskopf estimate for the half-life of the $E_\gamma = 231$ keV transition in ^{133}Xe is 1.8 μs for an $M2$ and 32 ms for an $E3$ transition. In ^{135}Ba the half-life corresponding to one Weisskopf unit is 1.1 μs for an $M2$ and 16 ms for an $E3$ transition. Assuming a pure $M2$ transition, the Weisskopf hindrance factors of the $J^\pi = 23/2^+$ isomers are $F_W = T_{1/2}^{\mathrm{exp}}/T_{1/2}^{\mathrm{W}} = 4800$ in ^{133}Xe and $F_W = 964$ in ^{135}Ba, compared to values of $F_W = 0.27$ and $F_W = 0.066$ for pure $E3$ transitions, respectively.

The experimental $B(M2)$ and $B(E3)$ values of the $23/2_1^+ \to 19/2_1^-$ decay in ^{133}Xe are $209(3) \times 10^{-6}$ and $1.7(16) \times 10^{-3}$ W.u., respectively. Calculations with the four interactions yield $B(M2)$ values, which overpredict the experimental result by factors of 3.2–8.1. The measured $E3$ admixture of the 231-keV transition is predicted at least one to two orders of magnitude too high. Only the $B(E3)$ value computed by the GCN50:82 interaction is in reasonable agreement with the measured one.

The calculations for ^{135}Ba yield 2.2–3.9 times larger $M2$ transition strengths compared to the experimental $M2$ transition strength $B(M2; 23/2^+ \to 19/2^-) = 1.053(40) \times 10^{-3}$ W.u. Moreover, the transition strength to the first excited $J^\pi = 19/2^-$ state is computed to be 2.277×10^{-3}, 1.607×10^{-3}, and 2.627×10^{-3} W.u. by the GCN50:82, SN100-KTH, and SN100PN interactions, respectively. The $B(E3)$ value of the 254-keV transition is overestimated by two orders of magnitude.

The calculated $B(M2)$ values depend on the choice of proton and neutron g factors. Calculations employing $g_l(\pi) = 1.13$, $g_s(\pi) = 4.04$, $g_l(\nu) = 0.02$, and $g_s(\nu) = -2.65$, taking into account core polarization and meson-exchange currents [74,75], change the $B(M2; 23/2^+ \to 19/2^-)$ values slightly to 1.679×10^{-3} W.u (SN100PN), 0.693×10^{-3} W.u (GCN50:82), and 1.771×10^{-3} W.u (SN100-KTH) in ^{133}Xe and similar values of 2.559×10^{-3} W.u (SN100PN), 4.029×10^{-3} W.u (GCN50:82), and 2.406×10^{-3} W.u (SN100-KTH) in ^{135}Ba.

The fact that the $M2$ transition operator is mainly assigned to a change in neutron configuration (cf. Fig 10) is also reflected in the proton A_p and neutron A_n amplitudes which serve as weighting factors for the proton and neutron contribution to the $M2$ matrix elements. For the GCN50:82 interaction, the A_p and A_n amplitudes are 0.032 and 0.251 in ^{133}Xe and 0.057, 0.463 in ^{135}Ba, respectively.

The shell-model calculations support a dominating $M2$ character for the $23/2^+ \rightarrow 19/2^-$ transitions. Calculating the ratio $B(M2)/B(E3)$ by using Eqs. (3) and (4) and solving for $|\delta|$ yields multipole-mixing ratios of 0.230, 0.068 (realistic SM), 0.098, 0.055 (SN100PN), 0.032, 0.013 (GCN50:82), and 0.158, 0.003 (SN100-KTH) for ^{133}Xe and ^{135}Ba, respectively. The values derived from the shell-model results are very similar to the experimentally determined $|\delta|$ values of 0.021(10) and 0.009(4). Moreover, the results support the smaller $E3$ admixture in ^{135}Ba compared to ^{133}Xe.

V. CONCLUSIONS

In summary, a detailed study of isomeric $J = 23/2^+$ states was performed in ^{133}Xe and in ^{135}Ba. Their half-lives of $T_{1/2} = 8.64(13)$ ms in ^{133}Xe and $T_{1/2} = 1.06(4)$ ms in ^{135}Ba close a gap along the $N = 79$ isotones. Measurements of the multipole-mixing ratio and internal-conversion coefficient of the 231-keV transition in ^{133}Xe and the 254-keV transition in ^{135}Ba yield a dominant $M2$ character. The experimentally determined $B(M2)$ and $B(E3)$ transition strengths are compared to the results of large-scale shell-model calculations employing the realistic SM, GCN50:82, SN100PN, and SN100-KTH interactions. In particular, interactions with improved and corrected monopole parts, i.e., GCN50:82, show a good agreement with the experimental findings. A detailed inspection of the evolution of proton and neutron decompositions along the $N = 79$ chain provide insight into the changing nuclear structure. The neutron configuration $\nu(h_{11/2}^{-2}d_{3/2}^{-1})$ is responsible for the isomeric character of the $23/2^+$ states. The different shell-model calculations follow the measured $B(M2)$ systematics as function of proton filling in the $gdsh$ orbitals along the $N = 79$ isotones. In particular, the agreement between calculated and experimental $B(M2)$ values improves with increasing proton number.

However, the systematics of the $N = 79$ isotonic chain still lacks some information. In 2013 a recoil-decay tagging experiment reported on three feeding transitions decaying into the isomeric $J^\pi = (23/2^+)$ state at $E_x = 2616$ keV in ^{139}Nd [3]. So far, there are no states observed that populate the $J^\pi = 23/2^+$ isomers in ^{131}Te and ^{135}Ba. In future, a similar measurement in both nuclei is of high interest to resolve those feeding patterns. There is a large disagreement between shell-model theory and experiment for the transition strength of the $23/2_1^+ \rightarrow 19/2_1^-$ decay in ^{131}Te, motivating new refined experiments.

Furthermore, despite a detailed knowledge of the high-spin regime in ^{137}Ce, no $J^\pi = 23/2_1^+$ isomer was reported to date. The hitherto known $23/2^+$ state disrupts the isotonic systematics and is unlikely an isomer. However, the 2490-keV state, decaying into the $19/2_2^-$ state, is a possible candidate for the expected isomer [14]. Further experiments should be performed to elucidate a possible onset of $J^\pi = 23/2_1^+$ isomerism in ^{137}Ce.

ACKNOWLEDGMENTS

We thank the IKP FN Tandem accelerator team for the professional support during the experiment. The research leading to these results has received funding from the German BMBF under Contract No. 05P12PKFNE TP4, from the European Union Seventh Framework Programme FP7/2007-2013 under Grant Agreement No. 262010 - ENSAR, from the Spanish Ministerio de Ciencia e Innovación under contract FPA2011-29854-C04, from the Spanish Ministerio de Economía y Competitividad under Contract No. FPA2014-57196-C5, and from the U.K. Science and Technology Facilities Council (STFC). L.K. and A.V. thank the Bonn-Cologne Graduate School of Physics and Astronomy (BCGS) for financial support. One of the authors (A. Gadea) has been supported by the Generalitat Valenciana, Spain, under the grant PROMETEOII/2014/019 and EU under the FEDER program.

[1] J. Genevey, J. A. Pinston, C. Foin, M. Rejmund, H. Faust, and B. Weiss, High spin isomers in ^{129}Sn and ^{130}Sb, Phys. Rev. C **65**, 034322 (2002).

[2] A. Astier, M. G. Porquet, Ts. Venkova, Ch. Theisen, G. Duchêne, F. Azaiez, G. Barreau, D. Curien, I. Deloncle, O. Dorvaux, B. J. P. Gall, M. Houry, R. Lucas, N. Redon, M. Rousseau, and O. Stézowski, High-spin structures of $^{124-131}$Te: Competition of proton- and neutron-pair breakings, Eur. Phys. J. **50**, 1 (2014).

[3] A. Vancraeyenest, C. M. Petrache, D. Guinet, P. T. Greenlees, U. Jakobsson, R. Julin, S. Juutinen, S. Ketelhut, M. Leino, M. Nyman, P. Peura, P. Rahkila, P. Ruotsalainen, J. Saren, C. Scholey, J. Sorri, J. Uusitalo, P. Jones, C. Ducoin, P. Lautesse, C. Mancuso, N. Redon, O. Stezowski, P. Désesquelles, R. Leguillon, A. Korichi, T. Zerrouki, D. Curien, and A. Takashima, Identification of new transitions feeding the high-spin isomers in ^{139}Nd and ^{140}Nd nuclei, Phys. Rev. C **87**, 064303 (2013).

[4] R. L. Lozeva, G. S. Simpson, H. Grawe, G. Neyens, L. A. Atanasova, D. L. Balabanski, D. Bazzacco, F. Becker, P. Bednarczyk, G. Benzoni, N. Blasi, A. Blazhev, A. Bracco, C. Brandau, L. Cáceres, F. Camera, S. K. Chamoli, F. C. L. Crespi, J.-M. Daugas, P. Detistov, M. De Rydt, P. Doornenbal, C. Fahlander, E. Farnea, G. Georgiev, J. Gerl, K. A. Gladnishki, M. Górska, J. Grębosz, M. Hass, R. Hoischen, G. Ilie, M. Ionescu-Bujor, A. Iordachescu, J. Jolie, A. Jungclaus, M. Kmiecik, I. Kojouharov, N. Kurz, S. P. Lakshmi, G. Lo Bianco, S. Mallion, A. Maj, D. Montanari, O. Perru, M. Pfützner, S. Pietri, J. A. Pinston, Zs. Podolyák, W. Prokopowicz, D. Rudolph, G. Rusev, T. R. Saitoh, A. Saltarelli, H. Schaffner, R. Schwengner, S. Tashenov, K. Turzó, J. J. Valiente-Dobón, N. Vermeulen, J. Walker, E. Werner-Malento, O. Wieland, and H.-J. Wollersheim, New sub-μs isomers in ^{125,127,129}Sn and isomer systematics of $^{124\text{-}130}$Sn, Phys. Rev. C **77**, 064313 (2008).

[5] A. Vogt, M. Siciliano, B. Birkenbach, P. Reiter, K. Hadyńska-Klęk, C. Wheldon, J. J. Valiente-Dobón, E. Teruya, N. Yoshinaga, K. Arnswald, D. Bazzacco, A. Blazhev, A. Bracco, B. Bruyneel, R. S. Chakrawarthy, R. Chapman, D. Cline, L. Corradi, F. C. L. Crespi, M. Cromaz, G. de Angelis, J. Eberth, P. Fallon, E. Farnea, E. Fioretto, C. Fransen, S. J. Freeman, B. Fu, A. Gadea, W. Gelletly, A. Giaz, A. Görgen, A. Gottardo, A. B.

Hayes, H. Hess, R. Hetzenegger, R. Hirsch, H. Hua, P. R. John, J. Jolie, A. Jungclaus, V. Karayonchev, L. Kaya, W. Korten, I. Y. Lee, S. Leoni, X. Liang, S. Lunardi, A. O. Macchiavelli, R. Menegazzo, D. Mengoni, C. Michelagnoli, T. Mijatović, G. Montagnoli, D. Montanari, C. Müller-Gatermann, D. Napoli, C. J. Pearson, Zs. Podolyák, G. Pollarolo, A. Pullia, M. Queiser, F. Recchia, P. H. Regan, J.-M. Régis, N. Saed-Samii, E. Şahin, F. Scarlassara, M. Seidlitz, B. Siebeck, G. Sletten, J. F. Smith, P.-A. Söderström, A. M. Stefanini, O. Stezowski, S. Szilner, B. Szpak, R. Teng, C. Ur, D. D. Warner, K. Wolf, C. Y. Wu, and K. O. Zell, High-spin structures in ^{132}Xe and ^{133}Xe and evidence for isomers along the N = 79 isotones, Phys. Rev. C **96**, 024321 (2017).

[6] B. Fogelberg, H. Mach, H. Gausemel, J. P. Omtvedt, and K. A. Mezilev, New high spin isomers obtained in thermal fission, in *The Second International Workshop on Nuclear Fission and Fission-Product Spectroscopy*, edited by G. Fioni, H. Faust, S. Oberstedt, and F.-J. Hambsch, AIP Conf. Proc. No. 447 (AIP, New York, 1998), p. 191.

[7] M. Ferraton, R. Bourgain, C. M. Petrache, D. Verney, F. Ibrahim, N. de Séréville, S. Franchoo, M. Lebois, C. Phan Viet, L. Sagui, I. Stefan, J. F. Clavelin, and M. Vilmay, Lifetime measurement of the six-quasiparticle isomer in ^{140}Nd and evidence for an isomer above the $19/2^+$ state in ^{139}Nd, Eur. Phys. J. A **35**, 167 (2008).

[8] Evaluated Nuclear Structure Data File (ENSDF), http://www.nndc.bnl.gov/ensdf.

[9] J. A. Pinston, C. Foin, J. Genevey, R. Béraud, E. Chabanat, H. Faust, S. Oberstedt, and B. Weiss, Microsecond isomers in ^{125,127,129}Sn, Phys. Rev. C **61**, 024312 (2000).

[10] C. T. Zhang, P. Bhattacharyya, P. J. Daly, Z. W. Grabowski, R. H. Mayer, M. Sferrazza, R. Broda, B. Fornal, W. Królas, T. Pawlat, D. Bazzacco, S. Lunardi, C. Rossi Alvarez, and G. de Angelis, Yrast excitations in $A = 126-131$ Te nuclei from deep inelastic ^{130}Te+^{64}Ni reactions, Nucl. Phys. A **628**, 386 (1998).

[11] J. Ludziejewski and H. Arnold, High-spin levels in ^{137,139}Ce and ^{139,141}Nd evidence for hole-core coupling, Z. Phys. A **281**, 287 (1977).

[12] M. Müller-Veggian, Y. Gono, R. M. Lieder, A. Neskakis, and C. Mayer-Böricke, High-spin states and isomers in ^{136,137,138}Ce, Nucl. Phys. A **304**, 1 (1978).

[13] S. J. Zhu, L. Y. Zhu, M. Li, C. Y. Gan, M. Sakhaee, L. M. Yang, R. Q. Xu, Z. Zhang, Z. Jiang, G. L. Long, S. X. Wen, X. G. Wu, and X. A. Liu, High spin states and a collective oblate band in ^{137}Ce, Phys. Rev. C **62**, 044310 (2000).

[14] T. Bhattacharjee, S. Chanda, A. Mukherjee, S. Bhattacharyya, S. Kumar Basu, S. S. Ghugre, U. D. Pramanik, R. P. Singh, S. Muralithar, N. Madhavan, J. J. Das, and R. K. Bhowmik, Multi-quasiparticle bands in ^{137}Ce, Phys. Rev. C **78**, 024304 (2008).

[15] M. Müller-Veggian, H. Beuscher, D. R. Haenni, R. M. Lieder, A. Neskakis, and C. Mayer-Böricke, Investigation of high-spin states in ^{138,139}Nd, Nucl. Phys. A **344**, 89 (1980).

[16] M. A. Cardona, G. de Angelis, D. Bazzacco, M. De Poli, and S. Lunardi, High spin levels in ^{141}Sm, Z. Phys. A **340**, 345 (1991).

[17] M. Lach, P. Kleinheinz, J. Blomqvist, A. Ercan, H. J. Hähn, D. Wahner, R. Julin, M. Zupancic, F. Cigoroglu, and G. de Angelis, Shell model yrast states in the $N = 79$ nuclei ^{141}Sm and ^{143}Gd, Z. Phys. A **345**, 427 (1993).

[18] M. Sugawara, H. Kusakari, Y. Igari, K. Myojin, D. Nishimiya, S. Mitarai, M. Oshima, T. Hayakawa, M. Kidera, K. Furutaka, and Y. Hatsukawa, Dipole and quadrupole cascades in the yrast region of ^{143}Gd, Eur. Phys. J. A **1**, 123 (1998).

[19] R. M. Lieder, T. Rząca-Urban, H. J. Jensen, W. Gast, A. Georgiev, H.M. Jäger, E. van der Meer, Ch. Droste, T. Morek, D. Bazzacco, S. Lunardi, R. Menegazzo, C. M. Petrache, C. Rossi Alvarez, C. A. Ur, G. de Angelis, D. R. Napoli, Ts. Venkova, and R. Wyss, From highly to superdeformed shapes: Study of ^{143}Gd, Nucl. Phys. A **671**, 52 (2000).

[20] R. A. Meyer, F. F. Momyer, J. H. Landrum, E. A. Henry, R. P. Yaffe, and W. B. Walters, Levels of odd-mass Xe populated in the beta decay of ^{129}Cs, and ^{133}I, Phys. Rev. C **14**, 1152 (1976).

[21] Y. Khazov, A. Rodionov, and F. G. Kondev, Nuclear data sheets for $A = 133$, Nucl. Data Sheets **112**, 855 (2011).

[22] T. Lönnroth, J. Kumpulainen, and C. Tuokko, One- and three-quasiparticle states in ^{127,129,131,133}Xe and their coexistence with band structures, Phys. Scr. **27**, 228 (1983).

[23] R. G. Wille and R. W. Fink, Activation cross sections for 14.8-MeV neutrons and some new radioactive nuclides in the rare earth region, Phys. Rev. **118**, 242 (1960).

[24] X. L. Che, S. J. Zhu, M. L. Li, Y. J. Chen, Y. N. U, H. B. Ding, L. H. Zhu, X. G. Wu, G. S. Li, C. Y. He, and Y. Liu, High-spin levels based on the $11/2^-$ isomer in ^{135}Ba, Eur. Phys. J. A **30**, 347 (2006).

[25] W. T. Cluff, High-Spin Structure of ^{134,135}Ba and ^{120}Te, Ph.D. thesis, Florida State University, 2008.

[26] S. Kumar, A. K. Jain, Alpana Goel, S. S. Malik, R. Palit, H. C. Jain, I. Mazumdar, P. K. Joshi, Z. Naik, A. Dhal, T. Trivedi, I. Mehrotra, S. Appannababu, L. Chaturvedi, V. Kumar, R. Kumar, D. Negi, R. P. Singh, S. Muralithar, R. K. Bhowmik, and S. C. Pancholi, Band structure and shape coexistence in $^{135}_{56}$Ba$_{79}$, Phys. Rev. C **81**, 067304 (2010).

[27] S. Akkoyun *et al.*, AGATA – Advanced GAmma Tracking Array, Nucl. Instrum. Methods Phys. Res. A **668**, 26 (2012).

[28] A. M. Stefanini, L. Corradi, G. Maron, A. Pisent, M. Trotta, A. M. Vinodkumar, S. Beghini, G. Montagnoli, F. Scarlassara, G. F. Segato, A. De Rosa, G. Inglima, D. Pierroutsakou, M. Romoli, M. Sandoli, G. Pollarolo, and A. Latina, The heavy-ion magnetic spectrometer PRISMA, Nucl. Phys. A **701**, 217 (2002).

[29] L. Corradi, S. Szilner, G. Pollarolo, D. Montanari, E. Fioretto, A. M. Stefanini, J. J. Valiente-Dobón, E. Farnea, C. Michelagnoli, G. Montagnoli, F. Scarlassara, C. A. Ur, T. Mijatović, D. Jelavić Malenica, N. Soić, and F. Haas, Multinucleon transfer reactions: Present status and perspectives, Nucl. Instrum. Methods Phys. Res. B **317, Part B**, 743 (2013).

[30] S. Szilner, C. A. Ur, L. Corradi, N. Marginean, G. Pollarolo, A. M. Stefanini, S. Beghini, B. R. Behera, E. Fioretto, A. Gadea, B. Guiot, A. Latina, P. Mason, G. Montagnoli, F. Scarlassara, M. Trotta, G. de Angelis, F. Della Vedova, E. Farnea, F. Haas, S. Lenzi, S. Lunardi, R. Marginean, R. Menegazzo, D. R. Napoli, M. Nespolo, I. V. Pokrovsky, F. Recchia, M. Romoli, M.-D. Salsac, N. Soić, and J. J. Valiente-Dobón, Multinucleon transfer reactions in closed-shell nuclei, Phys. Rev. C **76**, 024604 (2007).

[31] L. Netterdon, V. Derya, J. Endres, C. Fransen, A. Hennig, J. Mayer, C. Müller-Gatermann, A. Sauerwein, P. Scholz, M. Spieker, and A. Zilges, The γ-ray spectrometer HORUS and its applications for nuclear astrophysics, Nucl. Instrum. Methods. Phys. Res. A **754**, 94 (2014).

[32] A. Gadea, E. Farnea, J. J. Valiente-Dobón, B. Million, D. Mengoni, D. Bazzacco, F. Recchia, A. Dewald, Th. Pissulla,

W. Rother, G. de Angelis *et al.*, Conceptual design and infrastructure for the installation of the first AGATA sub-array at LNL, Nucl. Instrum. Methods Phys. Res. A **654**, 88 (2011).
[33] A. Wiens, H. Hess, B. Birkenbach, B. Bruyneel, J. Eberth, D. Lersch, G. Pascovici, P. Reiter, and H.-G. Thomas, The AGATA triple cluster detector, Nucl. Instrum. Methods Phys. Res. A **618**, 223 (2010).
[34] B. Bruyneel, B. Birkenbach, and P. Reiter, Pulse shape analysis and position determination in segmented HPGe detectors: The AGATA detector library, Eur. Phys. J. A **52**, 70 (2016).
[35] A. Lopez-Martens, K. Hauschild, A. Korichi, J. Roccaz, and J.-P. Thibaud, γ-ray tracking algorithms: a comparison, Nucl. Instrum. Methods Phys. Res. A **533**, 454 (2004).
[36] R. S. Kempley *et al.*, Cross Coincidences in the ^{136}Xe + ^{208}Pb deep-inelastic reaction, Acta Phys. Pol. B **42**, 717 (2011).
[37] M. Siciliano *et al.*, Neutron-rich nuclei in the vicinity of ^{208}Pb, LNL Annual Report 2014 **241**, 63 (2015), https://www.lnl.infn.it/~annrep/read_ar/2014/contributions/pdfs/063_B_127_B122.pdf.
[38] N. Saed-Samii, Lifetime measurements using the FATIMA array in combination with EXOGAM@ILL, Diplomarbeit, Universität zu Köln, 2013.
[39] I. Wiedenhöver, Computer code CORLEONE, 1997 (unpublished).
[40] I. Wiedenhöver, O. Vogel, H. Klein, A. Dewald, P. von Brentano, J. Gableske, R. Krücken, N. Nicolay, A. Gelberg, P. Petkov, A. Gizon, J. Gizon, D. Bazzaco, C. Rossi Alvarez, G. de Angelis, S. Lunardi, P. Pavan, D. R. Napoli, S. Frauendorf, F. Dönau, R. V. F. Janssens, and M. P. Carpenter, Detailed angular correlation analysis with 4π spectrometers: Spin determinations and multipolarity mixing measurements in ^{128}Ba, Phys. Rev. C **58**, 721 (1998).
[41] K. S. Krane and R. M. Steffen, Determination of the $E2/M1$ Multipole Mixing Ratios of the Gamma Transitions in ^{110}Cd, Phys. Rev. C **2**, 724 (1970).
[42] K. S. Krane, R. M. Steffen, and R.M. Wheeler, Directional correlations of gamma radiations emitted from nuclear states oriented by nuclear reactions or cryogenic methods, At. Data Nucl. Data Tables **11**, 351 (1973).
[43] O. Brandstädter, F. Girsig, F. Grass, and R. Klenk, Eine schnelle Transportautomatik zur Untersuchung kurzlebiger Kernzustände bis in den Millisekunden-Bereich, Nucl. Instrum. Meth. **104**, 45 (1972).
[44] W. G. Winn and D. D. Clark, Half-Life of Ba^{136m}, Bull. Am. Phys. Soc. **11**, 775 (1966).
[45] F. Ruddy and B. D. Pate, The decay of 0.3 sec Ba^{136m}, Nucl. Phys. **69**, 471 (1965).
[46] P. F. Fettweis and E. C. Campbell, Isomères nucléaires produits par les neutrons d'un réacteur, Nucl. Phys. **33**, 272 (1962).
[47] A. Hashizume, H. Kumagai, Y. Tendow, and T. Katou, A mechanical beam chopper system for the measurement of half-lives in the millisecond region, Nucl. Instrum. Meth. **119**, 209 (1974).
[48] H. F. Brinckmann, C. Heiser, and W. D. Fromm, Ein hochangeregter isomerer Kernzustand in ^{132}Xe, Nucl. Phys. A **96**, 318 (1967).
[49] H. R. Hiddleston and C. P. Browne, Nuclear data sheets for A = 132, Nucl. Data Sheets **17**, 225 (1976).
[50] A. G. Demin and Y. P. Kushakevich, New Isomers of Sc^{43}, In^{109}, and Xe^{125}, Sov. J. Nucl. Phys. **1**, 138 (1965).
[51] T. Kibédi, T.W. Burrows, M. B. Trzhaskovskaya, P. M. Davidson, and C. W. Nestor, Jr., Evaluation of theoretical conversion coefficients using BrIcc, Nucl. Instrum. Methods Phys. Res., Sect. A **589**, 202 (2008).
[52] S. Raman, A simple method for accurate measurements of total internal conversion coefficients, Nucl. Instrum. Methods **103**, 407 (1972).
[53] H. W. Taylor, B. Singh, and D. A. Viggars, Mixing parameters of gamma transitions in ^{214}Po, Phys. Rev. C **34**, 2322 (1986).
[54] K. Rezynkina, A. Lopez-Martens, and K. Hauschild, On the graphical extraction of multipole mixing ratios of nuclear transitions, Nucl. Instrum. Methods Phys. Res. A **844**, 96 (2017).
[55] B. A. Brown and W. D. M. Rae, The Shell-Model Code NuShellX@MSU, Nucl. Data Sheets **120**, 115 (2014).
[56] N. Shimizu, Nuclear shell-model code for massive parallel computation, "KSHELL", arXiv:1310.5431 [nucl-ph].
[57] E. Caurier, G. Martínez-Pinedo, F. Nowacki, A. Poves, and A. P. Zuker, The shell model as a unified view of nuclear structure, Rev. Mod. Phys. **77**, 427 (2005).
[58] L. Coraggio, A. Covello, A. Gargano, N. Itaco, and T.T.S. Kuo, Effective shell-model hamiltonians from realistic nucleon-nucleon potentials within a perturbative approach, Ann. Phys. (NY) **327**, 2125 (2012).
[59] L. Coraggio, A. Covello, A. Gargano, N. Itaco, and T. T. S. Kuo, Shell-model calculations and realistic effective interactions, Prog. Part. Nucl. Phys. **62**, 135 (2009).
[60] B. A. Brown, N. J. Stone, J. R. Stone, I. S. Towner, and M. Hjorth-Jensen, Magnetic moments of the 2_1^+ states around ^{132}Sn, Phys. Rev. C **71**, 044317 (2005).
[61] R. Machleidt, F. Sammarruca, and Y. Song, Nonlocal nature of the nuclear force and its impact on nuclear structure, Phys. Rev. C **53**, R1483 (1996).
[62] E. Caurier, F. Nowacki, A. Poves, and K. Sieja, Collectivity in the light xenon isotopes: A shell model study, Phys. Rev. C **82**, 064304 (2010).
[63] E. Caurier, F. Nowacki, and A. Poves, Shell Model description of the $\beta\beta$ decay of ^{136}Xe, Phys. Lett. B **711**, 62 (2012).
[64] C. Qi, Shell-model configuration-interaction description of quadrupole collectivity in Te isotopes, Phys. Rev. C **94**, 034310 (2016).
[65] C. Qi and Z. X. Xu, Monopole-optimized effective interaction for tin isotopes, Phys. Rev. C **86**, 044323 (2012).
[66] F. LeBlanc, L. Cabaret, E. Cottereau, J. E. Crawford, S. Essabaa, J. Genevey, R. Horn, G. Huber, J. Lassen, P. Lee, G. LeScornet, J. Lettry, J. Obert, J. Oms, A. Ouchrif, J. Pinard, H. Ravn, B. Roussiére, J. Sauvage, D. Verney, J. Pinard, L. Cabaret, G. Huber, R. Horn, J. Lassen, J. E. Crawford, J. K. P. Lee, J. Genevey, G. LeScornet, J. Lettry, and H. Ravn, Charge-radius change and nuclear moments in the heavy tin isotopes from laser spectroscopy: Charge radius of ^{132}Sn, Phys. Rev. C **72**, 034305 (2005).
[67] G. White, J. Rikovska, N. J. Stone, J. Copnell, I. S. Towner, A. M. Oros, K. Heyde, B. Fogelberg, L. Jacobsson, and F. Gustavsson, Magnetic dipole moments near ^{132}Sn: Measurement on isomeric $11/2^-$ states in odd-A ^{131}Te and ^{133}Te by NMR/ON, Nucl. Phys. A **640**, 322 (1998).
[68] J. M. Allmond, D. C. Radford, C. Baktash, J. C. Batchelder, A. Galindo-Uribarri, C. J. Gross, P. A. Hausladen, K. Lagergren, Y. Larochelle, E. Padilla-Rodal, and C.-H. Yu, Coulomb excitation of ^{124,126,128}Sn, Phys. Rev. C **84**, 061303 (2011).

[69] J. K. Hwang, A. V. Ramayya, J. H. Hamilton, D. Fong, C. J. Beyer, K. Li, P. M. Gore, E. F. Jones, Y. X. Luo, J. O. Rasmussen, S. J. Zhu, S. C. Wu, I. Y. Lee, M. A. Stoyer, J. D. Cole, G. M. Ter-Akopian, A. Daniel, and R. Donangelo, Half-life measurement of excited states in neutron-rich nuclei, Eur. Phys. J. A **25**, 463 (2005).

[70] A. Vogt, B. Birkenbach, P. Reiter, A. Blazhev, M. Siciliano, K. Hadyńska-Klęk, J. J. Valiente-Dobón, C. Wheldon, E. Teruya, N. Yoshinaga, K. Arnswald, D. Bazzacco, M. Bowry, A. Bracco, B. Bruyneel, R. S. Chakrawarthy, R. Chapman, D. Cline, L. Corradi, F. C. L Crespi, M. Cromaz, G. de Angelis, J. Eberth, P. Fallon, E. Farnea, E. Fioretto, S. J. Freeman, B. Fu, A. Gadea, K. Geibel, W. Gelletly, A. Gengelbach, A. Giaz, A. Görgen, A. Gottardo, A. B. Hayes, H. Hess, R. Hirsch, H. Hua, P. R. John, J. Jolie, A. Jungclaus, L. Kaya, W. Korten, I. Y. Lee, S. Leoni, L. Lewandowski, X. Liang, S. Lunardi, A. O. Macchiavelli, R. Menegazzo, D. Mengoni, C. Michelagnoli, T. Mijatović, G. Montagnoli, D. Montanari, C. Müller-Gatermann, D. Napoli, C. J. Pearson, L. Pellegri, Zs. Podolyák, G. Pollarolo, A. Pullia, M. Queiser, F. Radeck, F. Recchia, P. H. Regan, D. Rosiak, N. Saed-Samii, E. Şahin, F. Scarlassara, D. Schneiders, M. Seidlitz, B. Siebeck, G. Sletten, J. F. Smith, P.-A. Söderström, A. M. Stefanini, T. Steinbach, O. Stezowski, S. Szilner, B. Szpak, R. Teng, C. Ur, V. Vandone, D. D. Warner, A. Wiens, C. Y. Wu, and K. O. Zell, Isomers and high-spin structures in the $N = 81$ isotones ^{135}Xe and ^{137}Ba, Phys. Rev. C **95**, 024316 (2017).

[71] J. J. Valiente-Dobón, P. H. Regan, C. Wheldon, C. Y. Wu, N. Yoshinaga, K. Higashiyama, J. F. Smith, D. Cline, R. S. Chakrawarthy, R. Chapman, M. Cromaz, P. Fallon, S. J. Freeman, A. Görgen, W. Gelletly, A. Hayes, H. Hua, S. D. Langdown, I. Y. Lee, X. Liang, A. O. Macchiavelli, C. J. Pearson, Zs. Podolyák, G. Sletten, R. Teng, D. Ward, D. D. Warner, and A. D. Yamamoto, ^{136}Ba studied via deep-inelastic collisions: Identification of the $(\nu h_{11/2})^{-2}_{10+}$ isomer, Phys. Rev. C **69**, 024316 (2004).

[72] H. C. Pauli, K. Alder, and R. M. Steffen, The Electromagnetic Interaction in Nuclear Spectroscopy in *Advances in Electronics and Electron Physics*, edited by P. W. Hawkes (Academic Press, New York, 1975), chap. 2, p. 39.

[73] O. J. Roberts, C. R. Niţă, A. M. Bruce, N. Mărginean, D. Bucurescu, D. Deleanu, D. Filipescu, N. M. Florea, I. Gheorghe, D. Ghiţă, T. Glodariu, R. Lica, R. Mărginean, C. Mihai, A. Negret, T. Sava, L. Stroe, R. Şuvăilă, S. Toma, T. Alharbi, T. Alexander, S. Aydin, B. A. Brown, F. Browne, R. J. Carroll, K. Mulholland, Zs. Podolyák, P. H. Regan, J. F. Smith, M. Smolen, and C. M. Townsley, $E3$ and $M2$ transition strengths in $^{209}_{83}$Bi, Phys. Rev. C **93**, 014309 (2016).

[74] G. Jakob, N. Benczer-Koller, G. Kumbartzki, J. Holden, T. J. Mertzimekis, K.-H. Speidel, R. Ernst, A. E. Stuchbery, A. Pakou, P. Maier-Komor, A. Macchiavelli, M. McMahan, L. Phair, and I. Y. Lee, Evidence for proton excitations in ^{130,132,134,136}Xe isotopes from measurements of g factors of 2^+_1 and 4^+_1 states, Phys. Rev. C **65**, 024316 (2002).

[75] A. E. Stuchbery, Gyromagnetic ratios of excited states and nuclear structure near ^{132}Sn, in *XXXVI Brazilian Workshop on Nuclear Physics*, edited by M. H. Tabacniks, J. R. B. de Oliveira, and J. Marco, AIP. Conf. Proc. No. 1625 (AIP, New York, 2014), p. 52.